Design of a Gravity Compensation Actuator for Arm Assistance

Chen Tang

Thesis submitted to the Faculty of the
Virginia Polytechnic Institute and State University
in partial fulfillment of the requirements for the degree of

Master of Science
in
Mechanical Engineering

Alan T. Asbeck, Chair
Pinhas Ben-Tzvi
Robert G. Parker

Dec. 18th, 2017
Blacksburg, Virginia

Keywords: Gravity compensation, elastic elements, passive actuator, upper extremities assistance

Design of a Gravity Compensation Actuator for Arm Assistance

Chen Tang

(ABSTRACT)

This thesis presents the design, simulation, and evaluation of a passive, wearable, and human-scale actuator that includes pulleys and uses polymers for energy storage. Repetitive tasks such as packing boxes on an assembly line may require high strength movements of the shoulder, arm, and hand and may result in musculoskeletal disorders. With the objective to offset the weight of the arm and thereby lower the forces on the muscles in the shoulder and arm, this actuator is able to provide gravity compensation for the upper extremities of workers, if used in conjunction with an arm exoskeleton. The actuator is passive, meaning that it does not use motors or sensors, but instead creates a force on a cable that is a function of the displacement of the cable.

This thesis details the design of the actuator and the selection of an appropriate polymer for use with the actuator. To determine the best polymer for this application, tests were conducted on nine polymers to find their average Young's modulus and their hysteresis. A 90A abrasion-resistant polyurethane rubber belt was used in the final design due to its high modulus and low hysteresis. The final actuator design was tested in an Instron machine to validate its performance. During testing, the actuator provided 720N in extension and 530N in retraction, which are roughly 112% and 83% of the torque required to lift a human arm, respectively.

Design of a Gravity Compensation Actuator for Arm Assistance

Chen Tang

(GENERAL AUDIENCE ABSTRACT)

The development of industry increases productivity, and brings convenience to people's life, but in the meantime it also increases work-related illnesses. Based on such condition, mechanical devices such as exoskeletons can be applied to support arms of wearer to perform tasks for longer durations and with less effort. In this thesis, we present a wearable actuator that contains pulleys and polymer belts. With rather light weight and small size, the actuator is located on the waist of wearer, and connected to the arm exoskeleton by cable. As the arm moves, the polymer belts within the actuator will be stretched and counteract the effects of movements. All in all, the design of the actuator must be portable, light-weight and with simple design that can be sufficient to meet actual requirements.

Contents

List of Figures

List of Tables

Chapter 1

Introduction

1.1 Background

1.1.1 Motivation

Scientific development is supposed to bring more convenience to people's lives; it frees humankind of heavy labour and increases productivity. In recent years, industry progress revitalizes the economy and creates a large number of employment opportunities, but in the meantime also increases public awareness of increasing work-related illnesses and industrial accidents. According to researchers, musculoskeletal disorders have become the most common self-reported, work-related illnesses [7], which influence people's health and work efficiency in modern society. Among them, cumulative trauma disorders (CTD), also known as repetitive strain disorders (RSI), are the main causes. They include specific disorders such as carpal tunnel syndrome, cubital tunnel syndrome, and tendonitis of the wrist or hand [8], with which high force and high repetitiveness were generally positively associated [9]. Also, some studies indicate that RSI patients have objective signs of minor polyneuropathy [10]. Repeated exertions often cause such disorders in the hand-arm-shoulder region [7, 11, 12].

In conjunction with the increase in industrial injuries, there has been an increase in the number of devices to prevent workers from getting injured in the first place. There are many

mechanical devices that serve as possible solutions to reducing these injuries. One possibility is to have workers wear exoskeletons that support the arm, with the purpose of creating a gravity-less environment that reduces workload for arm motions. For example, Lift Assist Device V22-L is designed to help workers carry heavy load easily. It is able to reduce the potential risk of back injury [13]. Another possibility is using humanoid robots to potentially decrease the number of repetitive strain injuries through having robots perform repetitive tasks instead of people. Additionally, with the development of human society, more unknown territories are being explored. Some of these include hazardous environments like undersea operations and missions in emergency rescues [14]. In these environments, it may be useful to have robots do exploration or tasks instead of humans. These robotic systems may benefit from the use of arms, so they can manipulate objects in their environments.

Although these mechanical devices have different frameworks, many of them contain gravity compensation systems. Suitable gravity compensations for the manipulators have been developed to reduce control complexity, avoid energy consumption in places other than actuator torque demand, and lead to dynamic performance improvement [15–17]. The performance of robotic systems such as humanoid robots or exoskeletons contain serial kinematic chains whose behavior can be strongly influenced by the power supply structure. However, large amounts of power are consumed in resisting gravitational forces; using a gravity compensation device frees this power for other purposes. For these reasons, many examples can be found of robotic arms, arm rehabilitation devices, and arm exoskeletons that use gravity compensation mechanisms.

There are many robotic devices include gravity compensations for arm support. Shirata et al. discuss the design and evaluation of a gravity compensation mechanism for a humanoid robot [17], Morita et al. research gravity compensation in three dimensional space [16], and Ulrich et al. describe a passive mechanical gravity compensation for robot manipulators [15]. Gravity compensation is also used in designs such as the PR-1 personal robotics development platform [3], which can be used to improve the quality in industry and life, and the humanoid robot Baxter, which is designed for low volume, high mix production jobs [18]. The Baxter

robot has two seven degree of freedom arms, and uses gravity compensation to reduce the motor size and increase human safety [19].

Gravity compensation mechanisms can also be devised for rehabilitation devices that are mainly used to balance the weight of extremities and improve the actuator output efficiency. The uses of rehabilitation devices include active rehabilitation of people who have become paralyzed or impaired due to physical injuries, occupational injuries, sports injuries, and strokes [20–22]. They can provide therapies which have positive effects on patients. There are a variety of such devices, including Armin, a robotic arm that can be used to support a patient's arm during rehabilitation [23], which increases the training intensity for the patients through using the robotics to replace human labor. Other rehabilitation devices such as Freebal [1], RUPERT [24] were also developed for robotic assisted repetitive therapy.

Furthermore, gravity compensation can be applied in exoskeletons. Some of the exoskeletons are designed for industrial use, and are mainly used to improve efficiency and create better work conditions. The device called ShoulderX uses the stored energy from gas springs to support the upper extremities [25], and the lightweight wearable Levitate Airframe uses a gas spring to support the arm and transfer the weight of the upper arm and shoulder to the main body and support the arms of skilled workers [26]. And a gravity-balanced leg orthosis which can be used in clinical studies of subjects with leg impairment [27].

In this context, the development of a passive, portable actuator is specifically proposed that, in conjunction with an arm exoskeleton, has the purpose of providing gravity compensation to upper extremities. Specifically, we are investigating a new gravity compensation mechanism and the use of polymer springs as an energy storage device, which has not yet been explored in detail.

1.2 Contributions

This thesis provides the following contributions:

- The design and analysis of a specific structure that contains pulleys and polymer

springs to create gravity compensation passively when used in conjunction with a shoulder exoskeleton.

- The exploration of polymers as an energy-storage element for gravity compensation mechanisms, as opposed to metal or gas springs.
- The experimental evaluation of the constructed gravity compensation actuator, including measurements of its effectiveness and a discussion of its performance.

1.3 Thesis Organization

The design and development of the pulley-rubber passive actuator are discussed in this thesis. The actuator aims to provide enough energy for arm gravity compensation in conjunction with an arm exoskeleton (not developed in this thesis). Chapter 1 indicates the motivations as to why a new type of passive actuator is needed. Chapter 2 discusses the current gravity compensation systems. Chapter 3 contains the problem statement and corresponding solutions. In Chapter 4, the design analysis and optimization of the pulley-rubber structure are discussed in detail. Component development, 3D model construction, and polymer material selection are included in Chapter 5. Chapter 6 includes the testing results, simulations of the actuator, and the comparison of the results between both. In the end, Chapter 7 summarizes the entire work, provides discussions about the results and recommendations for actuator promotion.

Chapter 2

Literature Review

2.1 Literature Review

In the work that has gone towards the many different applications that all use gravity compensation techniques, a number of different mechanical solutions have been explored and designed. Passive gravity compensation indicates the method of using weight, spring, or other energy storage members to counteract the effects of gravity without motors and sensors. In this section we go into more detail about how these different arm mechanisms work and the particular energy storage elements used in them.

2.1.1 Gravity Compensation with a Spring and Beam

In the traditional method, with the help of assistance provided by elastic energy storage elements, mobile arm mechanisms are proposed to support limbs in any movements through gravity compensation [28]. Also, these devices can facilitate people who have extremity problems get used to daily activities [29].

A number of different devices have used a similar mechanism for gravity compensation: a spring and beam are fastened to a fixed surface with pin joints, such that they can move in the vertical plane. The other end of the spring is connected to a point on the beam. By choosing the spring constant and distances appropriately, this provides gravity compensation

to the beam or objects attached to the beam.

Two of these devices are for upper-extremity rehabilitation: the Freebal [1] and Dampace [30]. These were proposed to increase the training intensity for the patients and gravity compensation components within both devices were quite similar. The gravity compensation force were both produced from a spring beam (Figure 2.1) at the base of devices and used cabling to transmit the force to support the wrist and elbow in the sling. By adjusting the distance of spring beam, the value of cable force can be changed to support different weight of upper extremities.

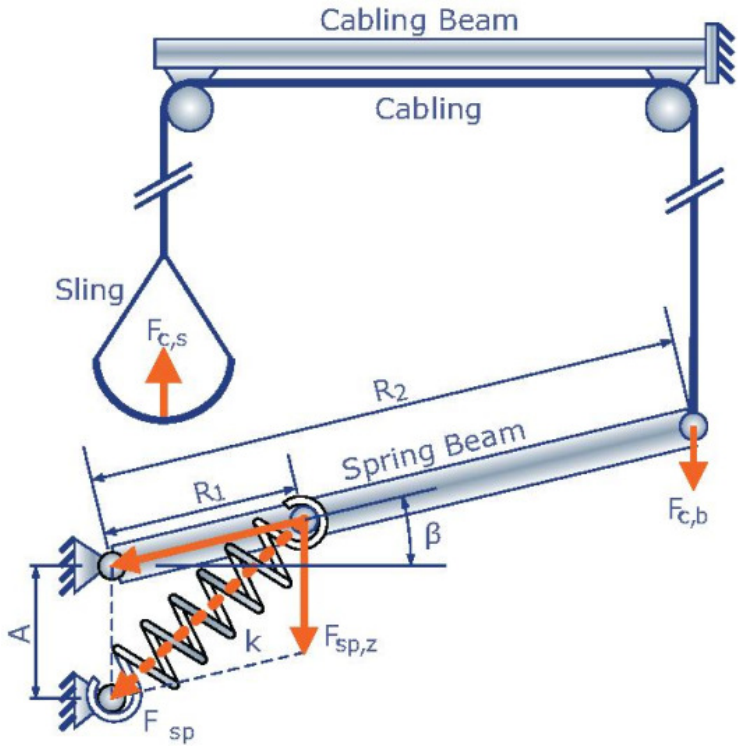

Figure 2.1: Spring and Beam Mechanism For Gravity Compensation [1]

Parallelogram link with springs is also a method developed for articulated manipulators and utilized for the reduction of gravity torque in each joint [16], the kinematic model is shown is Figure 2.2. The structure uses linear springs that were placed depending on kinematics to produce restoring force to counteract gravity force [2].

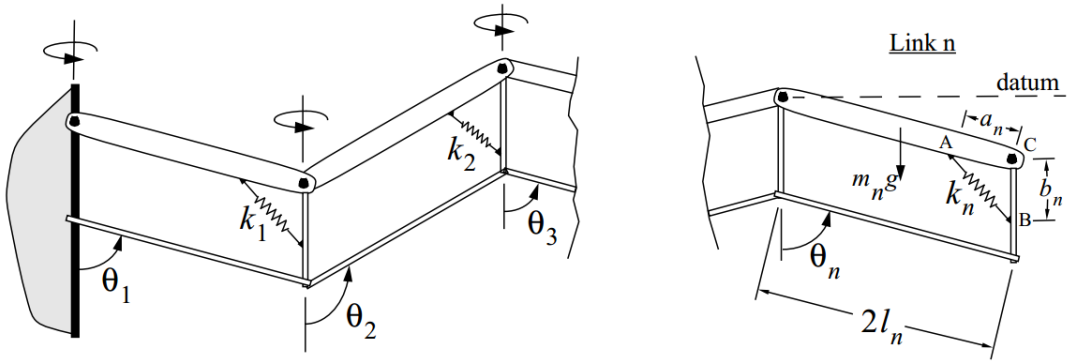

Figure 2.2: Gravity Compensation Method of Parallelogram Link with Springs. [2]

Another spring and parallelogram link mechanism is depicted in Figure 2.3, which is placed in PR-1 robot's arm segment to passively balance the arm weight and replace the use of joint motors. In this gravity compensation mechanism, spring is used to store energy and balance the force from distal link, connector bar can be used to transfer the elbow load to the shoulder location [3].

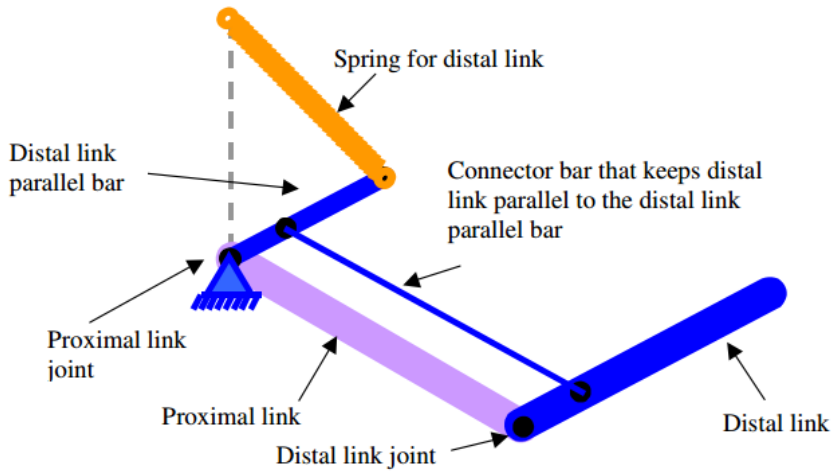

Figure 2.3: Parallelogram Mechanism Allows Gravity Compensation [3]

Similarly, other elastic elements can replace springs and work with parallelogram links.

For instance, a portable exoskeleton called JAECO WREX is able to balance upper extremity in space against the effects of gravity with the help of linear elastic band [31]. The device is designed quite close to human anatomy and enhances the arm movements of disabled patients. As depicted in Figure 2.4, the elastic bands are looped over two band spools on the humeral elevating link and forearm link. The elastic force produced by the bands counteracts the weight of upper extremity. This makes the number of bands are depending on the arm weight of different wearers and how much strength they need in the arm movements.

Figure 2.4: Child wears JAECO WREX.

2.1.2 Gravity Compensation with a Cam

In addition to the spring and parallelogram gravity compensation system, there are other hybrid structures. In this section, cam is treated as the main element within the gravity compensation mechanisms while working with other members such as springs or links. The first example is a cam type mechanism for gravity compensation [4]. As shown in Figure 2.5, an interior cam profile was designed to balance the weight force of an unbalanced rotating arm with weight (m). As the arm is rotating, pressures appear at the contact point of

follower and interior cam which creates a normal reaction force (N(q)). In the meantime, the counter balancing spring at the bottom is compressed and will create a resistance force acting on the follower shaft to balance the arm moving.

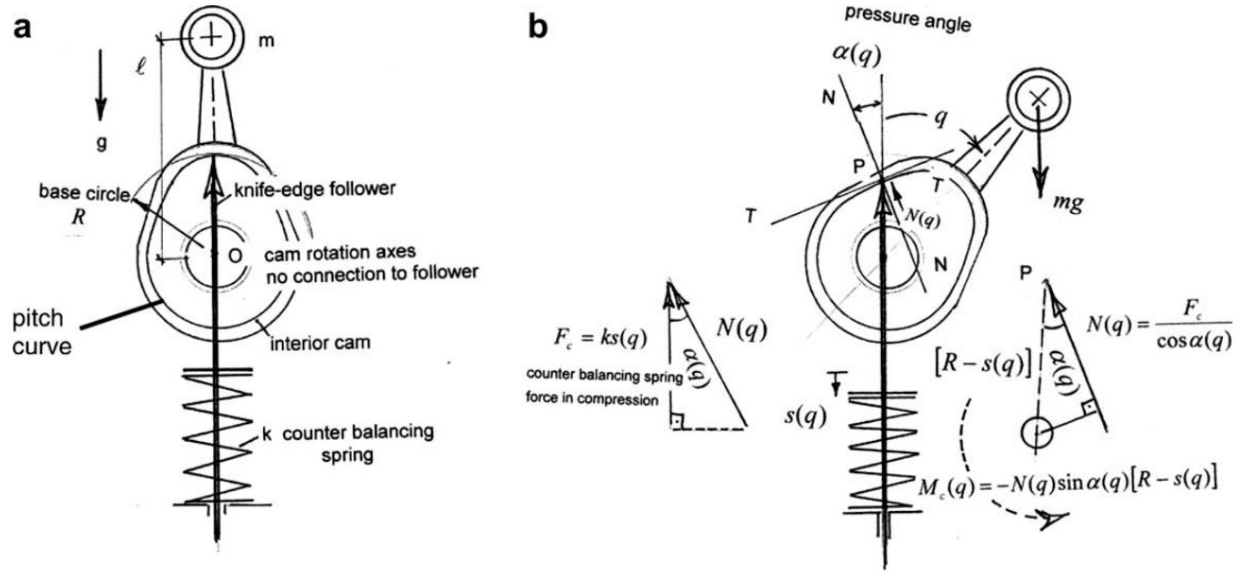

Figure 2.5: A Cam Mechanism for Gravity Compensation. [4]

Another gravity compensation mechanism called VGCM contained two types of linear springs and a follower to reduce actuator force mostly compensate for constant weight [5]. A prototype of the mechanism is shown in Figure 2.6. The main material is stainless steel with the weight of 7.5kg; two types of springs were placed with a 90° phase difference; a large follower with rotation axis inside and combined with a forward link. When there is force (mg) concentrated on the forward link, the gravity torque caused by (mg) will be compensated by torque generated by the spring forces.

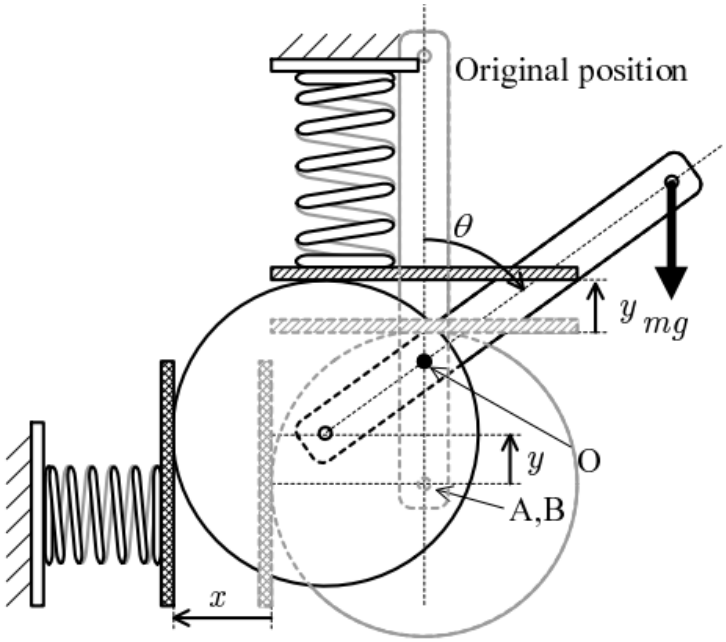

Figure 2.6: Gravity Compensation Mechanism Include Two Springs and a Cam [5]

Also, gravity compensations within several wearable industrial use exoskeletons contain cams. For instance, Levitate AIRFRAME [26], shoulderX [25], and Ekso Bionics Arm Support [32], as depicted in Figure 2.7, are wearable devices that can support arms of wearer to perform chest height to overhead tasks for longer durations and with less effort. These use compressed air springs mounted on the arm itself to provide gravity compensation in conjunction with a cam.

2.1.3 Gravity Compensation with pulleys

In this category, pulley is playing as the leading role in the gravity compensation mechanisms. For instance, the compensation mechanism for lower limb rehabilitation [6], depicted in Figure 2.8, contains springs, pulleys, and gears. It established a safer system with spring-pulley power supply structures embedded in the link body, which inspired the use of a pulley-spring structure and safe cover. When the joint shaft rotates angle θ, pulley 1 will rotate clockwise while pulley 2 rotate counter-clockwise by same angle. Crossing wire wrapped

(a) Levitate AIRFRAME

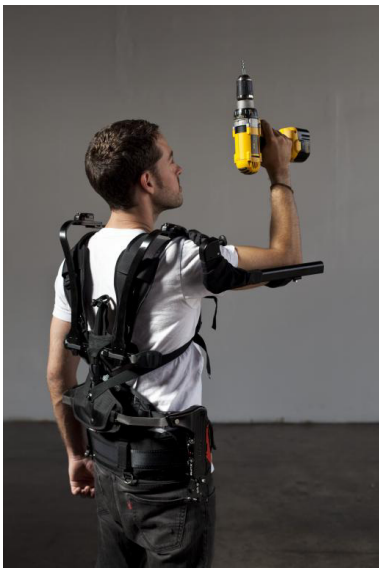

(b) shoulderX

(c) Ekso Bionics Exoskeleton

Figure 2.7: Exoskeletons Applied in Industry

around two pulleys with another spring hooked between them. Forces restored by the spring will cause a moment around the shaft joint that balances the gravitational moment.

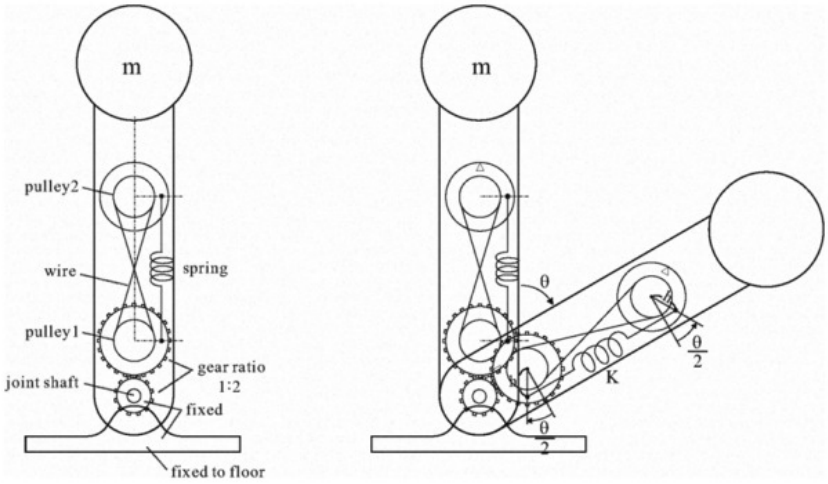

Figure 2.8: Gravity Compensation Mechanism from Paper [6]

Additionally, a passive, mechanical, and energy-conservative gravity compensation method was proposed for manipulator designs [15], which includes springs, cam, and bar. The weight of manipulators consume a big amount of energy while the development of motors are not good enough to ignore the influence from the structure within the system. This is why such methods are necessary. The method depicted in Figure 2.9 was developed for single joint compensation, which was made up of a spring-pulley structure. When there is force (m) concentrated on the end of the link, elastic force produced by the spring will cause a counter moment to balance the torque due to gravity. With known values (mg) and (L), variable suitable pulley radius r along with angle θ was specifically discussed, and the derivation of needed elastic coefficient k of the spring was achieved.

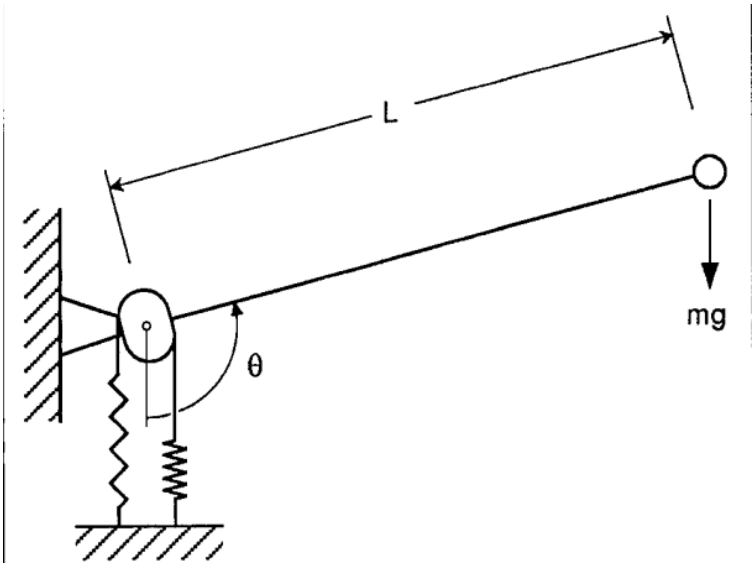

Figure 2.9: A cable/pulley/spring compensation method 2.9

2.2 Conclusion

There are many mechanisms for gravity compensation, including configurations of beams, cams, pulleys, and springs. In almost all of these prior examples, researchers used gas springs or metal springs to store energy, and used pulleys, gears, and links to transmit the power to support the upper extremities. Since these devices are typically made of steel, they may be relatively heavy. For wearable applications, we would like the entire system to be as light as possible. As such, this thesis explores the idea of using stretchable polymers (rubber) to store energy for gravity compensation instead of compressed air or metal springs. Also, each part of the polymer spring can be used as energy storage element, which reduces the space requirement for its elongation. This topic has not yet been researched in depth. We further investigate the development of a passive actuator that can effectively assist the human arm movements in work or daily life when in conjunction with a shoulder joint in an arm exoskeleton.

Chapter 3

Problem Statement and Proposed Solution

3.1 Motivation and Requirements

With the advancement of technology, interactions between humans and mechanisms have become more common. In this context, a suitable assistive actuator was created, since it could have a wide range of applications and could be used with a variety of devices. A primary demand for the actuator is that it can provide enough energy to reduce the amount of work that must be done by a human. In addition to satisfying the primary function, there are some other characteristics that depend on the actual use conditions. This actuator is aimed at people who are facing upper extremity problems because of work related repetitive movements [9]. From this point of view, a long lasting, portable actuator is preferred. Then, for the sake of easy operation, the actuator should be light-weight, reliable, and easy to use. Furthermore, in consideration of economics, the actuator must be accessible for operation and service, which means it is better to have a simple and passive mechanical design. In summary, a design of passive, assistive mechanical device is quite suitable for it can provide external forces directly and at the same time have a simple structure.

3.2 Design Approach

Based on these conditions, there were roughly three steps before determining the final version of the actuator during the design process. Our initial idea was to use a power supply structure on the back of a worker to provide enough energy to upper arms. Specific details for this idea are shown in Figure 3.1. On the horizontal rectangular aluminum piece (main piece), a plastic pulley and a small vertical rectangular aluminum piece (fixture end) are fixed on both ends and connected by a spring. The plastic pulley is placed coincident with the shoulder joint, so it is called the shoulder pulley. Also, a rectangular delrin piece is fixed with the shoulder pulley at one end, and attached with webbing to the upper arm to lift it. Along with the arm movements, the rotation of shoulder pulley will stretch the spring to produce elastic force. Furthermore, to prevent the whole device from shifting on the user, a waist belt is connected to the bottom end of a vertical aluminum piece.

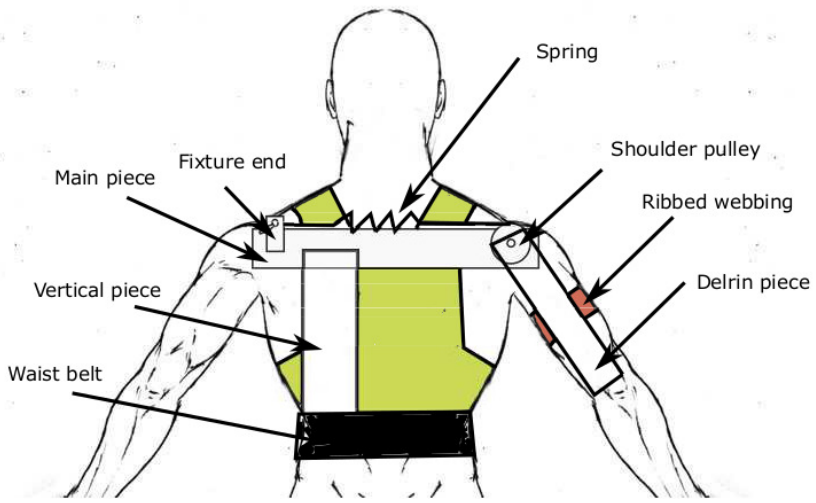

Figure 3.1: First Version of the Design

Initial testing showed that this design is able to provide good support for the upper extremity only when the arm moves in the frontal plane; it resists motion when the arm moves forward and backward. In addition, the whole device is too big and inconvenient. Therefore, a second plan was proposed. Rather than using one device which included a power

supply structure and arm assistance function, creating a small size and simplified actuator was more flexible and reduced the complexity. As shown in Figure 3.2, a portable power supply structure is placed at the lower back, connecting with the arm exoskeleton through the shoulder pulley and a Bowden cable. To satisfy all the requirements as discussed in the background section, a careful design of the power supply structure was quite important. This design and the associated analysis are the focus of the remainder of this thesis.

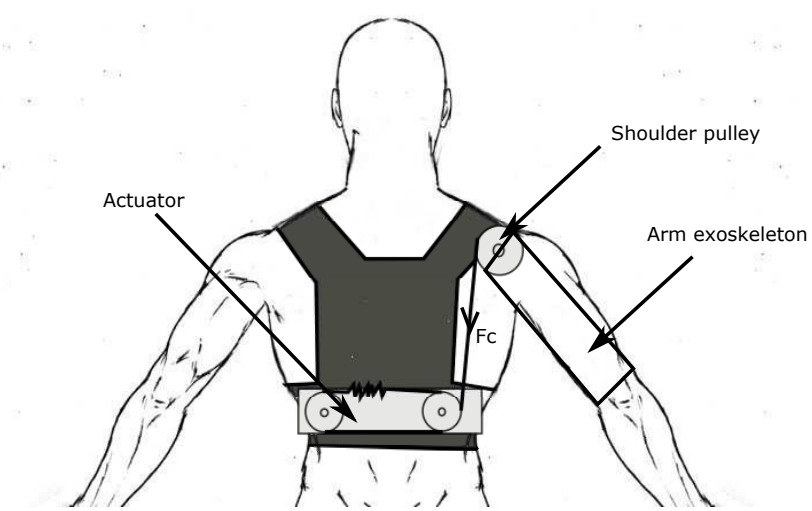

Figure 3.2: Second version of the design, which is the concept for the resulting solution.

In consideration of the actuator volume and output requirements, the energy storage system inside cannot be just a single spring as depicted in Figure 3.2. Following our analysis, the final structure of the actuator designed in this thesis is depicted in Figure 3.3b. The final design includes two pulleys with an elastic band surrounding them, and a cable wrapped around a third pulley that extends up to the shoulder. For the sake of human safety, the structure is enclosed inside an aluminum cover.

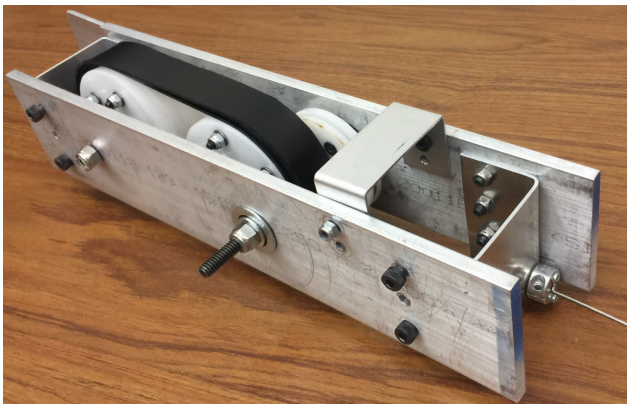

(a) The gravity compensation passive actuator developed in this thesis.

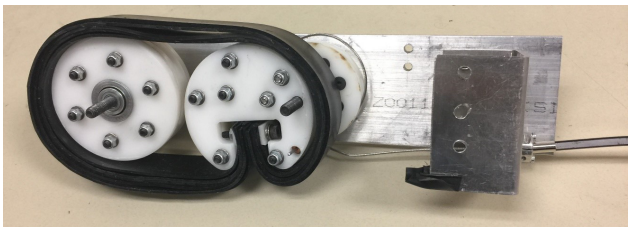

(b) The Actuator with Half of its Cover Removed

3.3 Hypotheses

Following our design ideas and literature review, we hypothesize that:

- A gravity-compensation structure based on elastomers as opposed to metal or gas springs will provide torques to support more than 50% of the arm's weight at the shoulder.
- A structure based on two rotating pulleys will combine with the nonlinear elastomer force-displacement relationship to create an appropriate torque-angle relationship to support the shoulder.

Chapter 4

Design Analysis of Gravity Compensation Structure

4.1 Introduction

The gravity compensation actuator is designed for weight lifting in conjunction with a wearable arm exoskeleton. One of the important goals of this design is to provide enough force to support the weight of the arm, while keeping the passive actuator small, light and portable. To realize this goal, this chapter discusses: analysis of the required shoulder torque to lift the whole arm; the design steps of pulley-rubber structure, including the rubber selection and the designs of the pulleys. The actuator is made up of a few parts, including: the rubber-pulley system, with the function of storing energy; the linkage part, which will be referred as the pulley-cable system and which is used to transmit the power from the actuator to the arm exoskeleton; and the safety stop piece, which is designed to prevent sudden power loss at the extreme condition where the combination of pulley 2 and 3 rotates over 180°. Analytical computational procedures which were used to verify the final design are also contained in this chapter.

4.2 Energy and Torque of Lifting Arm

Before determining the actuator structure, the calculations about the energy needed to lift the entire arm must be completed. In this analysis, we only consider the quasi-static motion of the arm, and aim to remove the effects of gravity from a person's arm. The shoulder pulley as depicted in Figure 4.1 has cable which comes out of the actuator wrapped around it, then the cable connects with an arm exoskeleton. The annotation r_{sp} means the radius of shoulder pulley, F_c means the cable force, and θ is the angle between the centerline of the arm and the vertical line. With the support from the actuator, an arm exoskeleton will offset the weight of the upper extremity when the arm rotates from $\theta = 0°$ to 180°. To hold the arm at some position, it is important to create a torque around the shoulder. Thus, kinematic analysis about the arm is necessary.

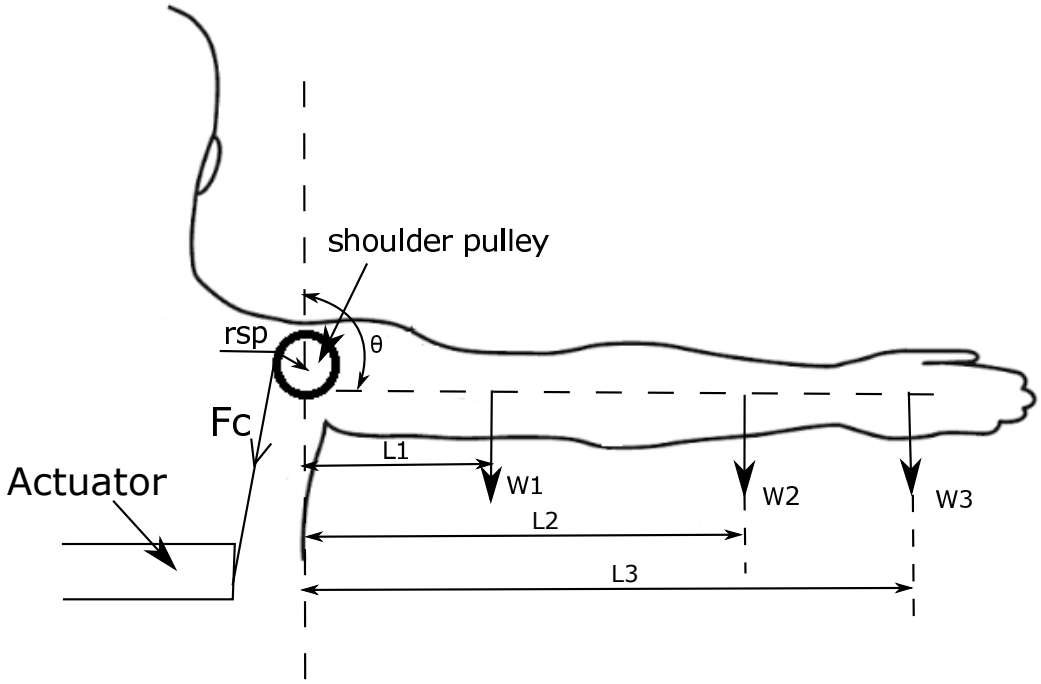

Figure 4.1: Free Body Diagram of Spreading Human Arm.

According to the segment weight data from de Leva [33], the weight of upper arm, forearm

Segment	Upper Arm	Forearm	Hand
Percentage of total body weight (%)	2.71	1.62	0.61
Length to shoulder (m)	L1=0.34	L2=0.27	L3=0.19
Weight (N)	W1=26.46	W2=15.88	W3=5.98

Table 4.1: Table of kinematic analysis parameters

and hand are 2.71%, 1.62%, and 0.6% of the total weight of a person. When achieving the free body diagram of human arm, analysis of the required torque and energy were finished to help find the values of cable force, and then the category of elastic material and the design of actuator were determined. According to the Table 4.1, torque acquired to lift the arm can be calculated as:

$$T_a = (L_1 \times w_1 + L_2 \times w_2 + L_3 \times w_3) \times \sin\theta \tag{4.1}$$

To achieve the exerted cable force F_c, apply the condition that all torques are balanced:

$$F_c \quad \times r_{sp} = T_a \tag{4.2}$$

$$F_c \quad = \frac{(L_1 \times w_1 + L_2 \times w_2 + L_3 \times w_3) \times \sin\theta}{r_{sp}} \tag{4.3}$$

$$F_c \quad = \frac{0.3408 \times 26.46 + 0.2699 \times 15.876 + 0.1937 \times 5.978}{r_{sp}} \tag{4.4}$$

$$F_c \quad = \frac{0.3408 \times 26.46 + 0.2699 \times 15.876 + 0.1937 \times 5.978}{r_{sp}} \tag{4.5}$$

What can be observed from the equations is the condition that the maximum force of cable provided by the actuator occurs when lifting the arm at the horizontal position, in other words, when $\theta = 90°$. The magnitude of the cable force can be adjusted by the selection of shoulder pulley. When the radius of shoulder pulley becomes bigger, the upper limit of cable

force is decreased, which would allow size reduction of actuator structure. For the sake of human body comfort and security, the radius of shoulder pulley must be kept in the range of 2 cm to 3 cm, thus, value 2.5 cm is chosen to be the radius of shoulder pulley and added in the Equation 4.3. Therefore, the maximum cable force can be calculated as:

$$F_{maxc} = \frac{(L_1 \times w_1 + L_2 \times w_2 + L_3 \times w_3) \times \sin 90^\circ}{0.025} = 642N \tag{4.6}$$

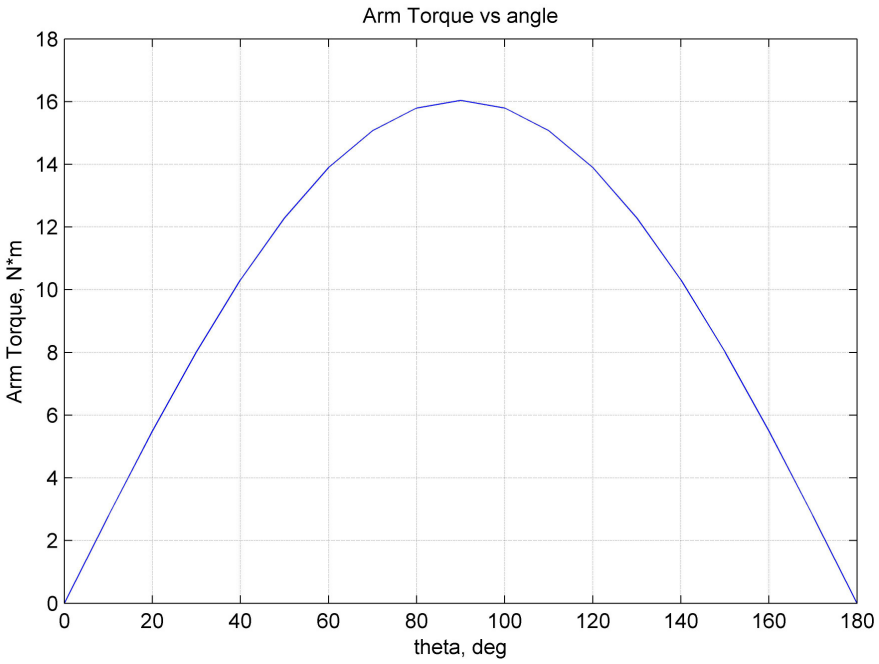

Figure 4.2: Arm Torque required to lift the arm.

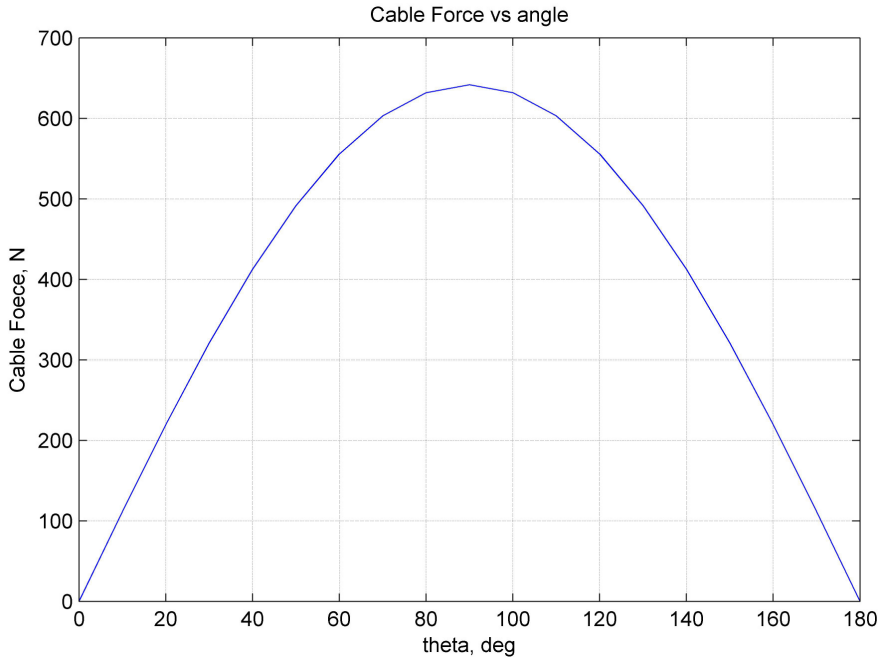

Figure 4.3: Cable Force required to lift the arm.

Cable force and arm torque can be calculated by using Equations 4.1 and 4.3, and how they vary along with the arm movements can be observed from Figure 4.2 and 4.3, which were analyzed in MATLAB. To meet the basic requirement, the maximum force that the actuator can supply should be comparable to the maximum cable force. Therefore, all the analyses discussed in this chapter will be used to determine the design of pulley-rubber structure.

The design of the actuator in the rest of this thesis assumes that a shoulder exoskeleton will have a circular pulley of radius r_{sp} as shown in Figure 4.1. The actuator will produce a force that, in combination with this pulley, will create an appropriate torque at the shoulder.

4.3 Design Analysis of the Gravity Compensation Actuator

4.3.1 Overall Design of Gravity Compensation Structure

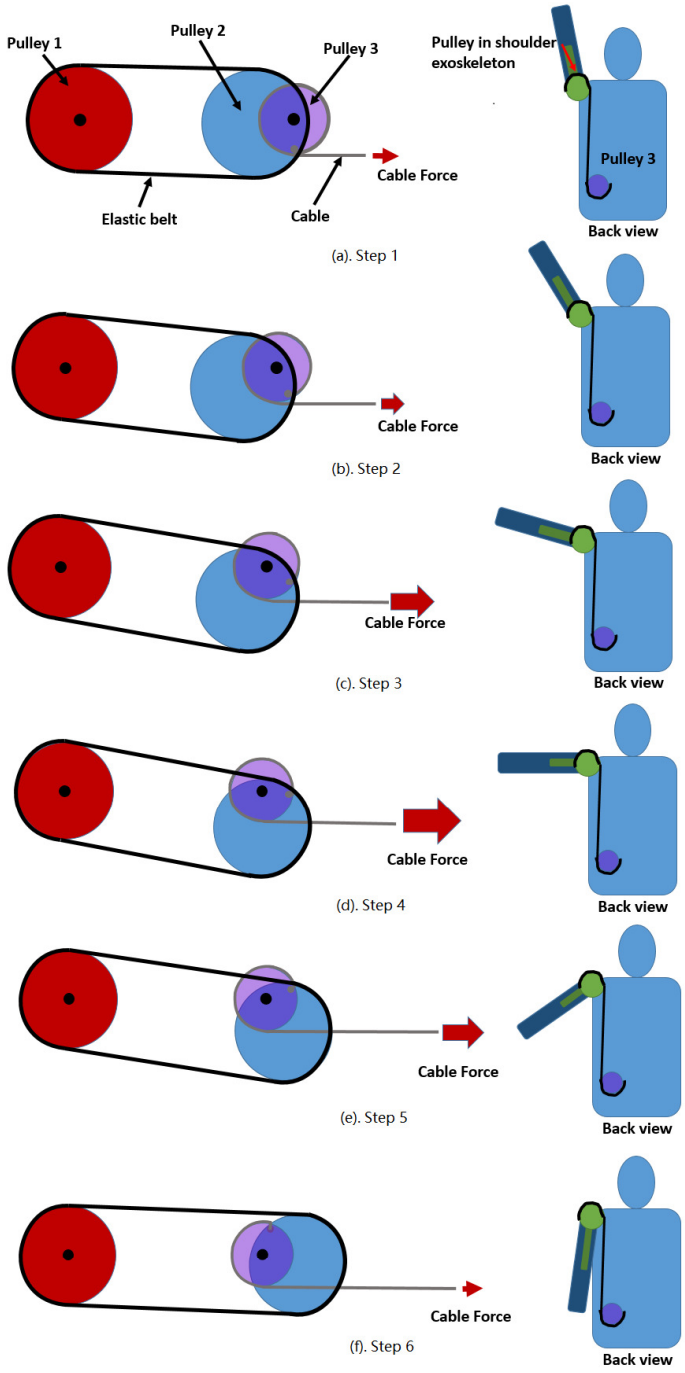

Figure 4.4: Principle of the Basic Structure within the Actuator

An overview of the proposed actuator is shown in Figure 4.4. Pulley 1 and pulley 2 are surrounded by an elastic belt; pulley 3 has a cable wrapped around it, and the cable comes out of the actuator from the right side and connects with an external arm exoskeleton. When there are arm movements, the cable will transmit the force to the actuator and lead the rotation of pulley 3. The elastic belt will be stretched to produce elastic force to balance the cable force. The image with Step 2 shows the actuator when the belt is stretched only a small amount, corresponding to the wearer's arm being nearly vertical up. Step 4 shows the belt is stretched and pulley 2 rotates 90°, corresponding to the wearer's arm being nearly horizontal. Step 6 shows the belt is stretched and pulley 2 rotates 180°, corresponding to the wearer's arm nearly drops.

4.3.2 Kinematic Analysis and Design Calculations

Since the main structure of the actuator is determined, the next step is to discuss the specific dimensions of each part. In this section we analyze these dimensions and the relationships between them. A geometric sketch of the structure is shown in Figure 4.5. To determine the belt length and required stiffness, main dimensions of the structure that must be chosen include the distance (D) between the centers of pulley 1 and pulley 3, the diameter (d) of pulley 1 and pulley 2, and the distance (L_0) between the centers of pulley 2 and pulley 3.

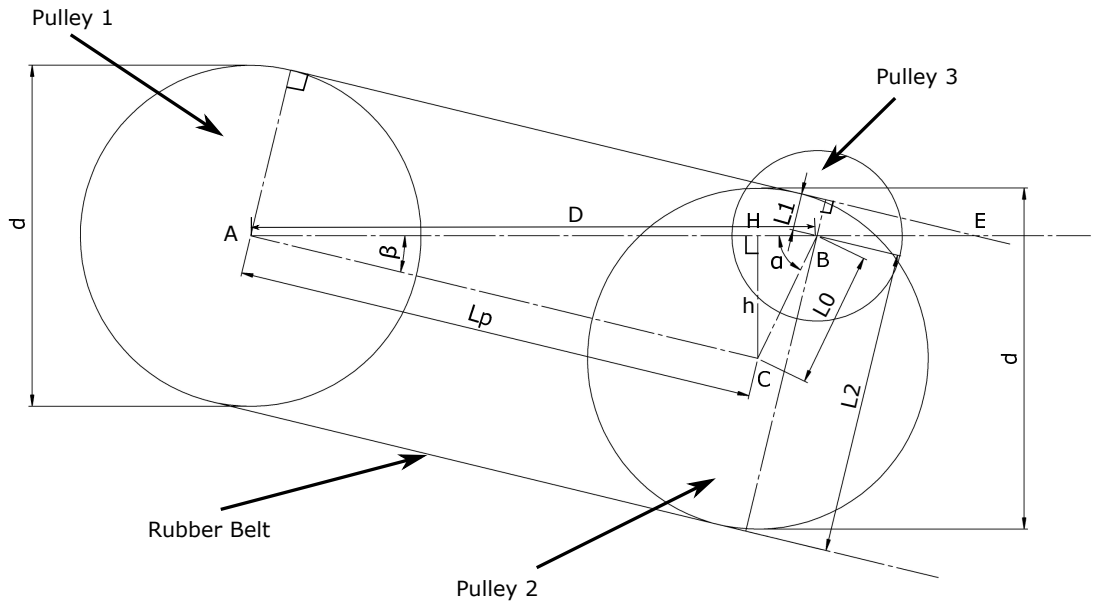

Figure 4.5: Sketch of Pulley-Rubber Structure

First, for the ease of calculation, it is appropriate to maintain the synchronous rotations of pulley 3 and the shoulder pulley. They were designed to have the same size, namely $r_3 = r_{sp} = 25mm$. A different size of this pulley could be used in the future for different sizes of people, so long as $r_3 = r_{sp}$. There are other four values (D), (d), (Lp), and (L_0) unknown. Among them, (Lp) will change along with the change of angle α and β during the rotation. Different value selections will influence the performance of the actuator. To choose the final values, the relationships between different variables can be determined through geometric analyses.

Figure 4.6 indicates the mathematical analysis of structure movements. (L_p) is the distance between centers of pulley 1 and pulley 2. Eq(4.7) indicates how the distance (L_p) changes along with the rotation angle α. Value (L_b) represents the total elastic belt length and can be calculated by Equation 4.11. Value (L_0) is the distance between BC. (D) is the distance between AB, which can be represented by the pulley 1 diameter (d) plus L_0 and plus l_{gap}. l_{gap} is a fixed, artificially set value that represents the shortest interval between pulley 1 and pulley 2 to create a buffer zone. Minimize the value of l_{gap} is able to minimize

the total actuator length, and 9 mm is chosen as the value in case of manufacturing errors.

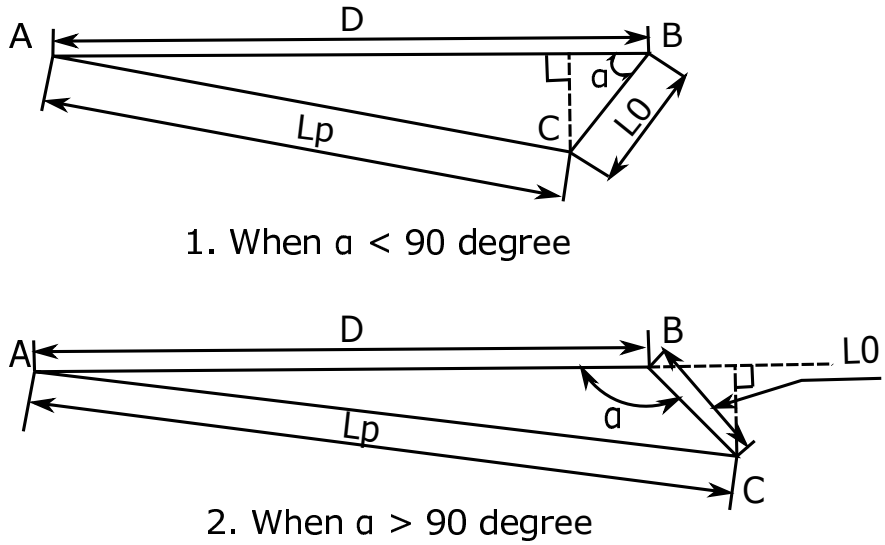

Figure 4.6: Mathematical Analysis of Structure Movements.

$$L_p = \sqrt{(D - L_0 \times \cos(\alpha))^2 + (L_0 \times \sin(\alpha))^2} \tag{4.7}$$

$$D = d + l_{gap} + L_0 \tag{4.8}$$

$$L_p = \sqrt{((d + l_{gap} + L_0) - L_0 \times \cos\alpha)^2 + (L_0 \times \sin\alpha)^2} \tag{4.9}$$

$$L_{max} = (L_0 + d) \times 2 + l_{gap} \tag{4.10}$$

$$L_b = d \times \pi + 2 \times L_p \tag{4.11}$$

To find out how the parameters influence the actuator functions, kinematic analyses are needed. According to the sketch in Figure 4.7, we apply the condition that all torques are balanced, then derived equations below:

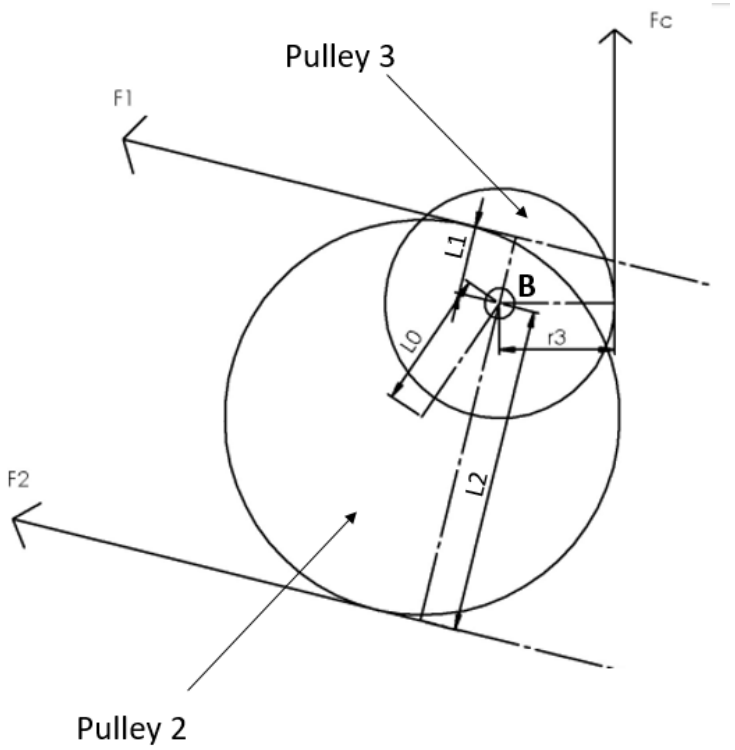

Figure 4.7: Free Body Diagram of Combination of Pulley 2 and 3.

$$F_c \quad \times r_3 + F_1 \times L_1 = F_2 \times L_2 \tag{4.12}$$

$$F_e \quad = F_1 = F_2 \tag{4.13}$$

$$F_e \quad = \frac{F_c \times r_3}{L_2 - L_1} \tag{4.14}$$

$$k \quad = \frac{F_e}{\Delta L_b} \tag{4.15}$$

$$\tag{4.16}$$

Equation 4.14 and 4.15 indicated how the needed cable force influenced the requirements of the belt elastic force and the selection of materials. F_c is the cable force, F_1 and F_2 are the elastic force of the belt, and $(\triangle L_b)$ is the increased length of belt during the stretch.

$$\sin\beta = \frac{h}{L_p} = \frac{L_0 \times \sin\alpha}{L_p} \tag{4.17}$$

$$sin\beta = \frac{r}{AE} \quad AE = \frac{r}{sin\beta} \tag{4.18}$$

$$AB = AE - BE, \quad BE = AE - AB, \; AB = D \tag{4.19}$$

$$F_e = \frac{F_c \times r_3}{L_2 - L_1} \tag{4.20}$$

$$\sin\beta = \frac{L_1}{BE} = \frac{L_1}{AE - AB} \tag{4.21}$$

$$L_1 = \sin\beta \times (AE - AB) = \frac{L_0 \times \sin\alpha}{L_p} \times [\frac{r \times L_p}{L_0 \times \sin\alpha} - D] \tag{4.22}$$

$$L_1 + L_2 = d, \quad L_2 - L_1 = d - 2 \times L_1 \tag{4.23}$$

$$L_2 - L_1 = d - \frac{2 \times L_0 \times \sin\alpha}{L_p} \times [\frac{r \times L_p}{L_0 \times \sin\alpha} - D] = \frac{2 \times D \times L_0 \times \sin\alpha}{L_p} \tag{4.24}$$

$$\triangle L_b = L_b(\alpha) - L_b(\alpha = 0^\circ) = 2 \times L_p - 2 \times (D - L_0) \tag{4.25}$$

$$k = \frac{F_e}{\triangle L_b} = \frac{F_c \times r_3}{(L_2 - L_1) \times \triangle L_b} = \frac{F_c \times r_3 \times L_p}{(L_p - D + L_0) \times 4 \times D \times L_0 \times \sin\alpha} \tag{4.26}$$

$$F_c = \frac{4 \times k \times D \times L_0 \times \sin\alpha \times (L_p - D + L_0)}{r_3 \times L_p} \tag{4.27}$$

The preceding equations show the derivation of the relationship between the various values and how they change along with the rotation of pulleys 2 and 3. Equation 4.26 and 4.27 indicate how values (d) and (L_0) influence the output force of the actuator and the needed elastic coefficient k to balance the arm torque.

4.3.3 Analysis of how the structure size impacts belt spring constant

Given the kinematic relationships of the structure, we next analyze how these variables impact the required spring constant of the rubber belt.

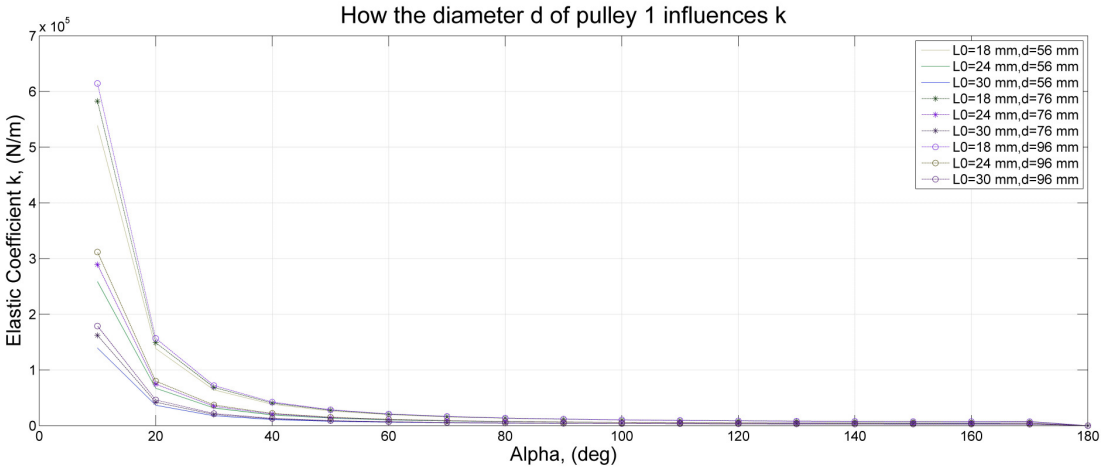

Figure 4.8: How Diameter d Influences Needed Belt k

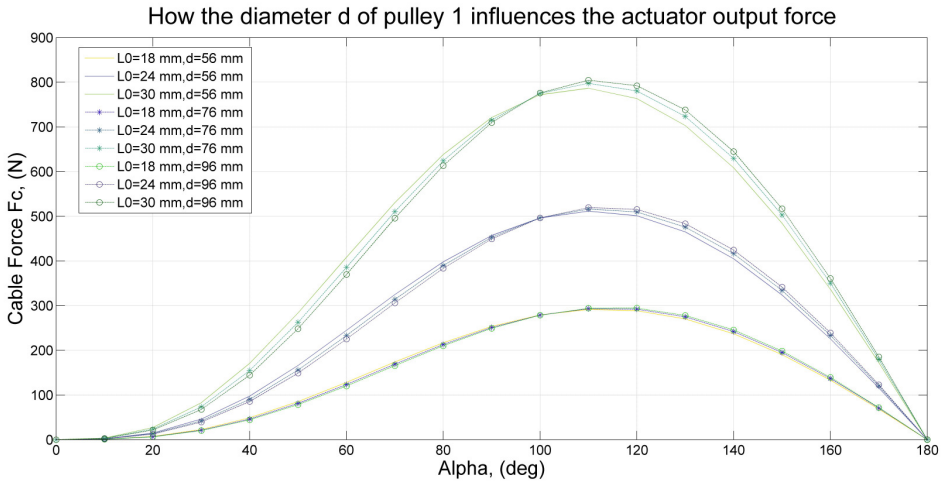

Figure 4.9: How Diameter d Influences Actuator Output Force, k=4550 N/m

Figure 4.8 and 4.9 indicate how value (d) influences the output force of the actuator F_c and the required elastic coefficient k. Three values $d = 56, 76, 96$ mm were substituted into Equation 4.26 and 4.27 with corresponding fixed values $L_0 = 18, 24, 30$ mm. In the pictures, calculated results implied that value d only has a small effect on k and F_c. As d gets bigger, the needed k gets larger and can produce a larger F_c value at a slightly smaller angle α.

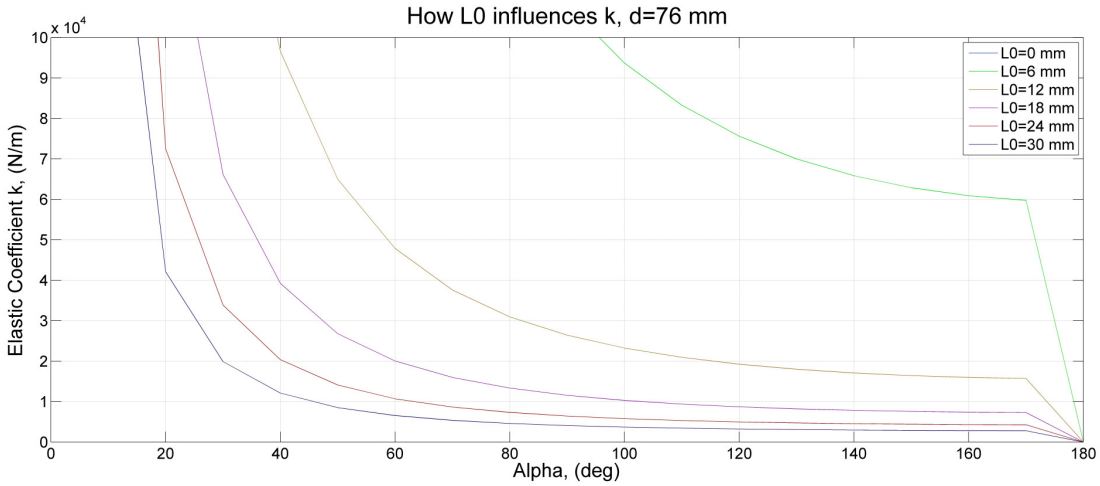

Figure 4.10: How L_0 Influences Needed Belt k

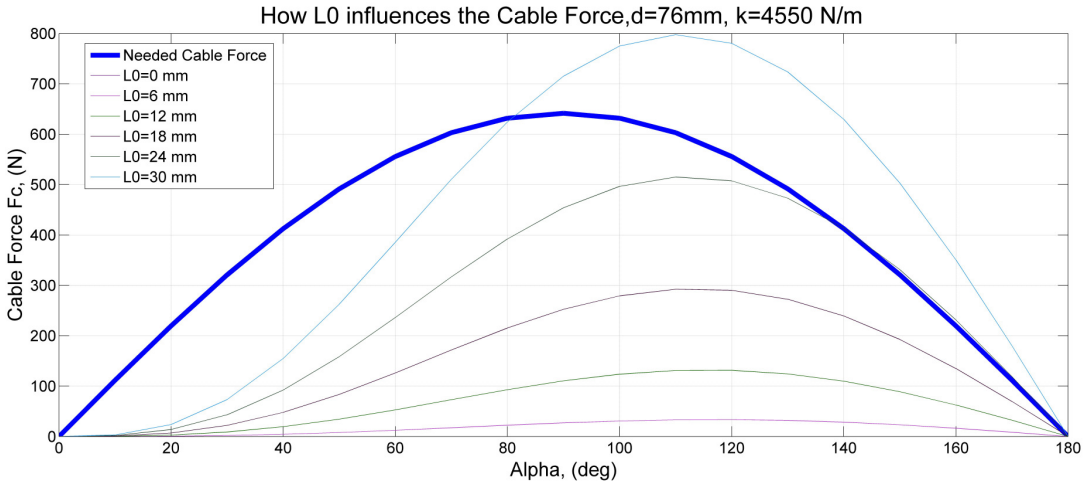

Figure 4.11: How L_0 Influences Actuator Output Force, $k = 4550N/m$

L_0 is the distance between the centers of pulley 2 and pulley 3. Figure 4.10 and 4.11 indicated how L_0 influenced the output force of the actuator F_c and the needed elastic coefficient k with a fixed value d=76mm. In the pictures, calculated results implied that L_0 has a strong influence on k and Fc. As L_0 gets bigger, the needed k gets much smaller and can produce a larger F_c value.

4.3.4 Analysis of how the structure size impacts belt lengths

Figure 4.12 and Figure 4.13 indicate how L_0 influences the belt length. When L_0 gets larger, the initial belt length will increase and the total strain will become larger during the working process (when α rotates from 0° to 180°).

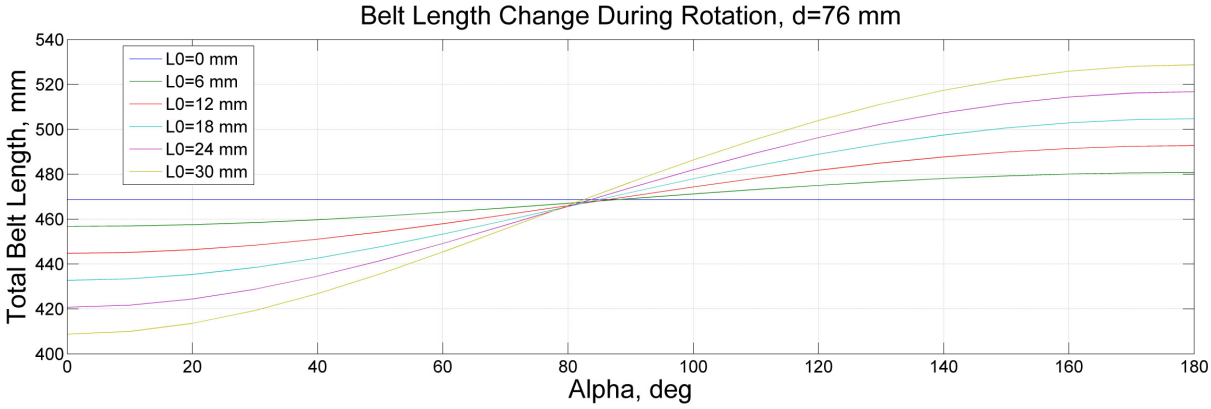

Figure 4.12: How L_0 Influences The Rubber Belt Length

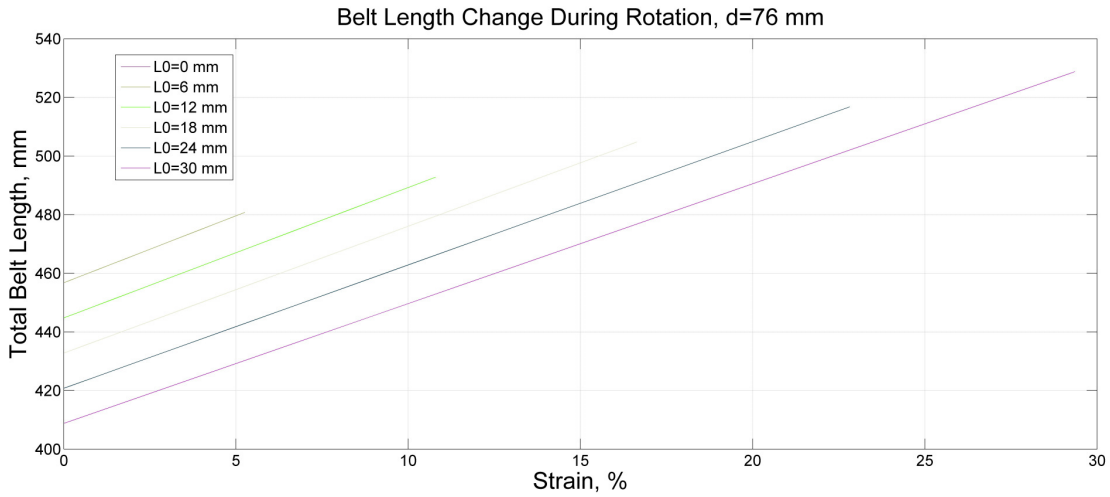

Figure 4.13: How L_0 Influences the Stretched Belt Length

4.3.5 Validation of Derived Equations

After completing the kinematic analysis of the force and torque, Equation 4.14 indicates the relationship between elastic force and other different dimensions. Cable force and the radius of pulley 3 are known, since both values of numerator are decided, the difference in length between L_1 and L_2 becomes the key factor that influences the elastic force.

In order to validate the derived equations, simulations were performed in SOLIDWORKS using a 2D drawing. Table 4.2 shows the simulation result of how different parameters change during the rotation process. The simulation used the dimensions from the sketch of pulley-rubber structure in Figure 4.16. Ideal k values to balance the cable force within the range of $\alpha = 0°$ *to* $180°$ were represented in Figure 4.14, which were achieved by substituting the data from Table 4.2 into the Equation 4.14 and 4.15. If the belt installed inside the actuator has the ideal k values, the output force of the actuator can exactly match the needed cable force as calculated in Figure 4.2. However, due to the fact that the shape of the curve resulting form the basic structure with 3 pulleys and the belt has a small output force at low α values, in this region, a very large required k is computed. In reality, k value depends on the material properties of the belt and will vary only slightly as stretched. As will be

Rotation angle, α°	Rubber stretched length ΔL_b mm	Perpendicular distance L1, mm	Perpendicular distance L2, mm	Difference value L2-L1=ΔL, mm
0	0	38.00	38.00	0.00
10	1.22	31.00	45.00	14.00
20	4.82	24.50	51.50	27.00
30	10.54	18.89	57.11	38.22
40	18.04	14.41	61.59	47.18
50	26.88	11.15	64.85	53.70
60	36.64	9.08	66.92	57.84
70	46.94	8.11	67.89	59.78
80	57.4	8.12	67.88	59.76
90	67.7	8.97	67.03	58.06
100	77.58	10.55	65.45	54.90
110	86.78	12.75	63.25	50.50
120	95.14	15.46	60.54	45.08
130	102.48	18.60	57.40	38.80
140	108.64	22.08	53.92	31.84
150	113.56	25.83	50.17	24.34
160	117.12	29.78	46.22	16.44
170	119.28	33.86	42.14	8.28
180	120	38.00	38.00	0.00

Table 4.2: Table of Parameter Variation during Rotation Simulation.

seen in Figure 5.16 in Chapter 5.3.1, polymer spring has a nonlinear k that is larger at small deflections, making those materials closer to the desire k than a metal spring.

These values in Table 4.2 were then compared to the computed values from the derived equations in Chapter 4.3.2 to verify the accuracy of the derived equations. The comparisons of simulated results and the equation results are depicted in Figure 4.15, which imply that the derived equations were correct.

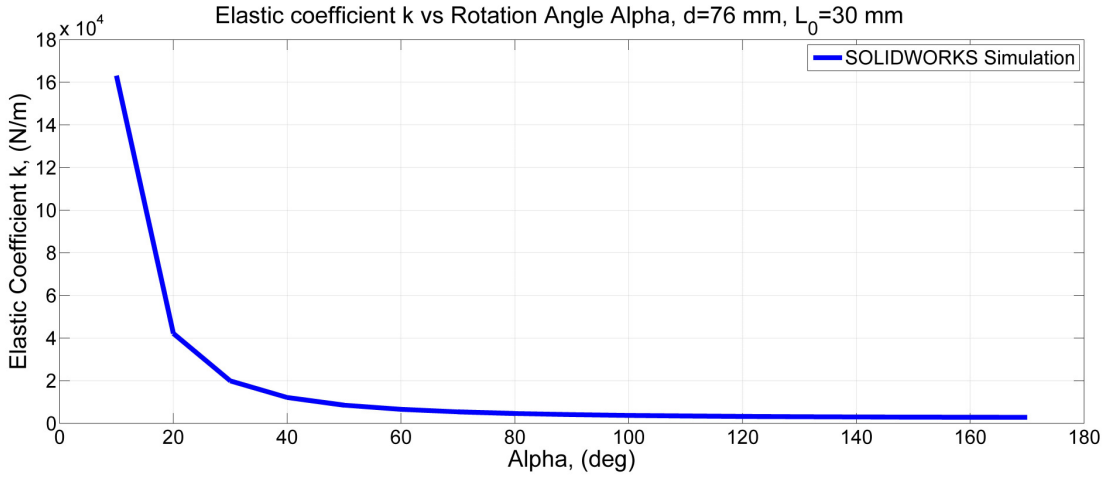

Figure 4.14: Simulated Ideal Elastic Coefficient during Rotation Process.

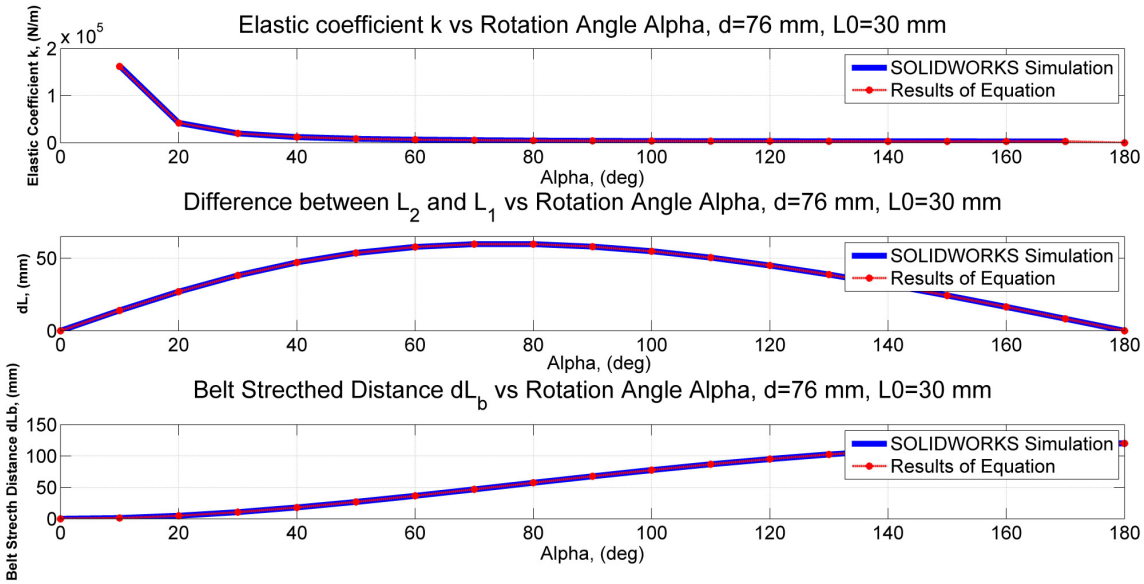

Figure 4.15: Results Comparison of Simulation and Equations, $d = 76$ mm $L_0 = 30$ mm.

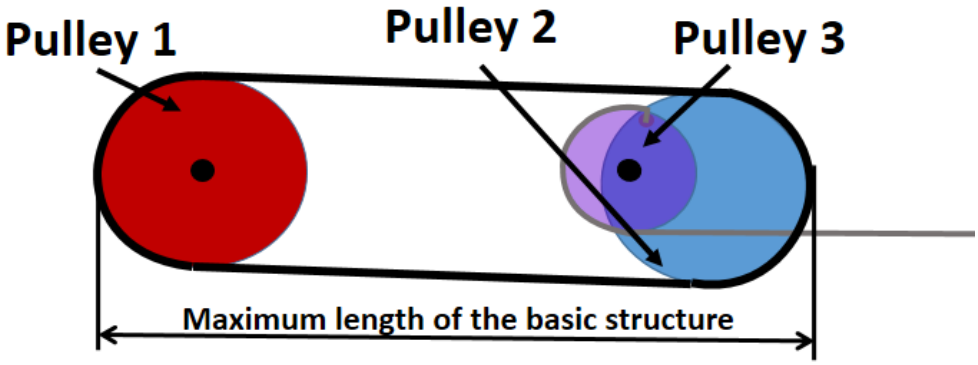

L0 (mm)	d (mm)	Maximum length of the basic structure (mm)
18	52	149
24	64	185
30	76	221
36	88	257
42	100	293

Table 4.3: Table of How L_0 and d Values Influence the Actuator Size.

4.3.6 Selection of Final Actuator Dimensions

As designed in Figure 4.5, pulley 1 and pulley 2 have the same diameter (d). Also, for the sake of tightening pulley 2 and 3, a 1/4" inch screw will be used at point (B) to fix the combination. Thus, the equation $L_0 + l_b \leq d$ is determined, where l_b is the distance between point (B) to the edge of pulley 2 to secure the combination. In consideration of the 1/4" inch screw at point (B), $l_b \geq 8mm$. We would like to size the actuator so it can fit on the wearer's torso. To achieve this, the size of the actuator can be roughly restricted to be less than 320 mm × 150 mm × 100 mm. The maximum length of the basic structure occurs when the combination of pulley 2 and pulley 3 rotates nearly 180°. At this point, the entire structure has width $2 \times (L_0 + d) + l_{gap}$, where l_{gap} is the distance between pulley 1 and pulley 2 when $\alpha = 0°$. For the rest of this design, we chose $l_{gap} = 9$ mm. After comparing the L_0 and d values in Table 4.3, $d = 76$ mm, $D = 115$ mm, and $L_0 = 30$ mm were chosen to be the dimensions. A structure with these specific values is shown in Figure 4.16.

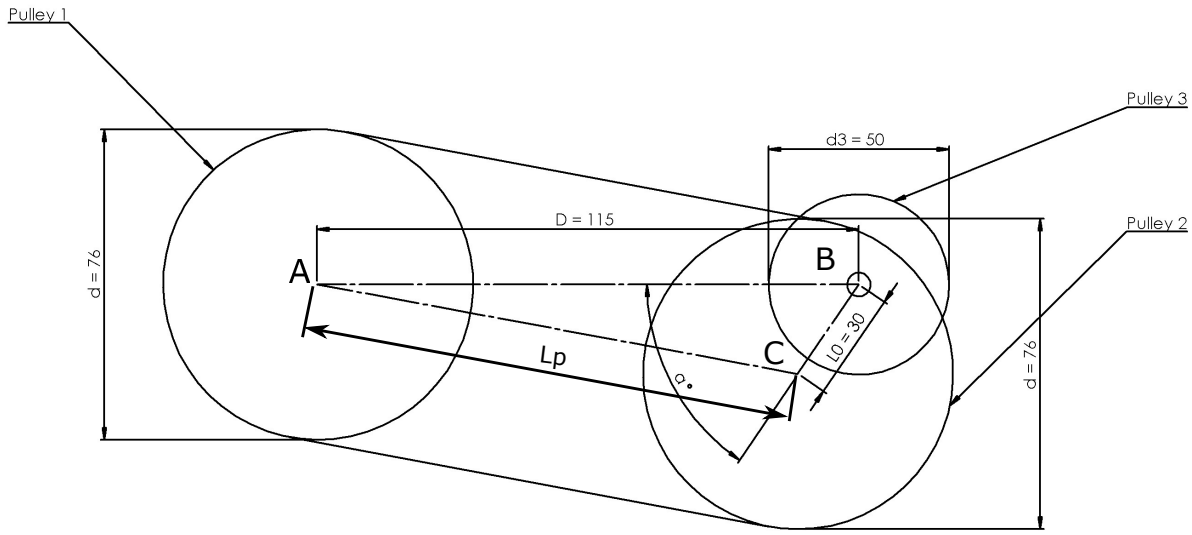

Figure 4.16: Sketch of Pulley-Rubber Structure with Specific Values.

4.3.7 Elastic Coefficient Selection

To identify further information of pulley-rubber structure, data from Table 4.2 can be used to calculate the elastic coefficient k, where α is the rotation angle of pulley 2. Substituting the value $\triangle L$ in Equation 4.14 and 4.15, the elongation range of rubber belt is between 0 *to* $4L_0$, namely 0 to 120 mm. Figure 4.14 shows the results of k values which can meet all the kinematic requirements at any condition during the rotation process. The structure requires a nonlinear spring. However, the ideal k value before rotating 80° is too large and there are no general rubber materials that can satisfy the requirement. Instead, a better solution is choosing the elastic coefficient k that can make the arm balanced around the horizontal position ($\alpha = 90°$). Two ways can be used to help determine the value.

$$When \quad \alpha \quad = 90°,\ L_2 - L_1 = 0.058mm \tag{4.28}$$

$$F_{e90} \quad = \frac{642N \times 0.025m}{0.058m} = 272.77N \tag{4.29}$$

$$k_{90} = \frac{F_{e90}}{\triangle x} = \frac{272.77}{0.0677} = 4029.1 N/m \tag{4.30}$$

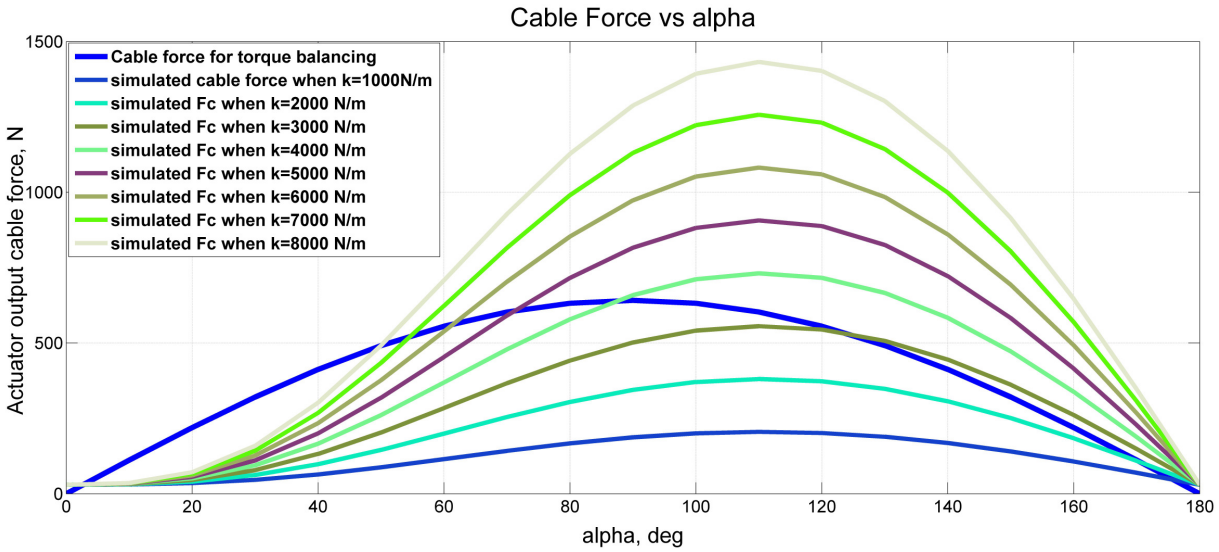

Figure 4.17: Comparison between desired cable force and simulated cable force for the proposed mechanism.

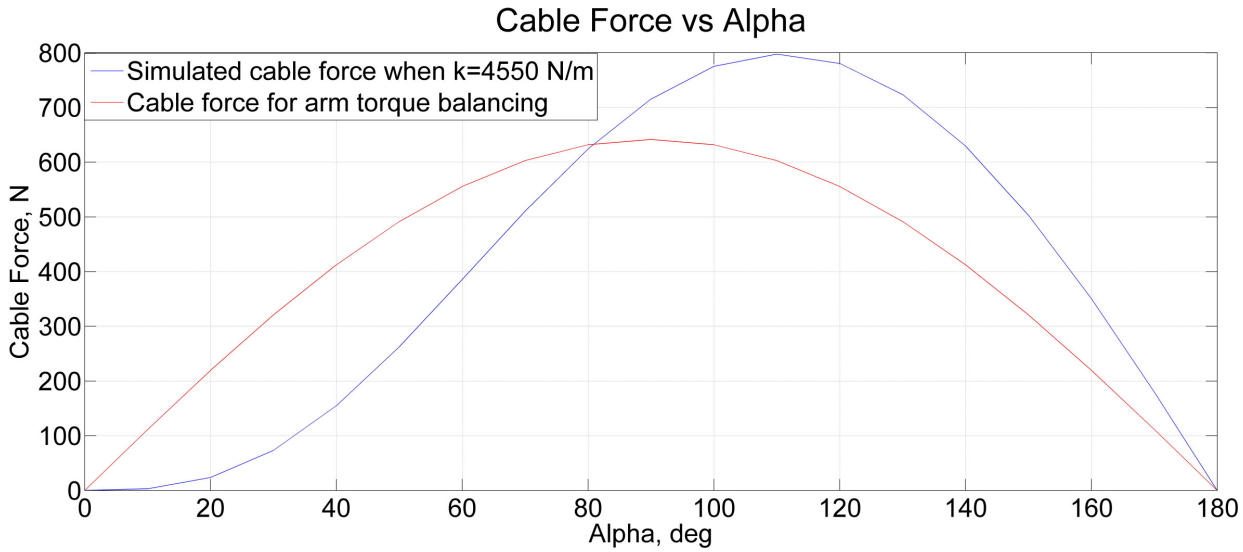

Figure 4.18: k= 4550 N/m, Comparison between desired cable force and simulated cable force for the proposed mechanism.

The calculated results from Equation 4.30 indicate that to make the arm balance in the horizontal position, the selection of elastic coefficient k must be bigger than 4030 N/m. In addition, we selected eight values that increase in sequence from 1000 to 8000 N/m evenly, substituted the data set in Equation 4.14 to achieve the simulated cable force, and then compared the simulations with the needed cable force. The contrast plot in Figure 4.17 implies a rough predication that when k is chosen between 4000 N/m to 5000 N/m, the actuator can provide enough force to make the arm stable between 70° to 90°. To specifically justify the assumption, k=4550 N/m was selected, and the comparison between the simulated cable force with the needed cable force is shown in Figure 4.18. This shows that the actuator is strong enough to support the arm when the rotation angle $\alpha = 80°$.

All the basic dimensions of the structure are now determined and the analysis of the elastic coefficient k was completed. The reasons why it is appropriate to use an elastic belt instead of a metal spring can now be discussed in detail. First, the elongation of the elastic object was set to be 120 mm. Different from a belt, when using a spring as the elastic object there cannot be interference between the spring and pulleys, which will cause the size of the actuator to increase. Second, the analysis about k indicated that an non-linear elastic object is preferred and to maintain the arm stable around horizontal line, the k value at least should be 4030 N/m (23 lbs./inch). On the other hand, to prevent the elastic object breaking, the selected object must be able to bear the maximum stretched force near 640 N. After searching the products from the Mcmaster, the suitable springs made of steel or piano wire were found to not meet the small size and light weight requirements. This led to the investigation of using rubber materials to provide energy storage.

All in all, the existence of reasonable k values indicates the assigned dimensions about the pulley-rubber structure are feasible.

4.3.8 Methods to Match the Actuator Output with the Needed Cable Force

The goal of the whole design is about developing an useful actuator for arm gravity compensation. However, the former discussions indicate that there are differences between the actuator output and the needed cable force at different angles. For example, comparing the simulated cable force with the needed cable force as shown in Figure 4.18, the simulated actuator force is very low at values of $\alpha < 40°$, and it is higher than the required force for values of $\alpha > 90°$. In this plot, the maximum difference between the two curves is 259 N and occurs when $\alpha \approx 40°$. Another way to quantify the difference is to compute the root mean square (RMS) of the difference between the curves, namely

$$RMS = \sqrt{\frac{1}{N}\sum_{i=1}^{N}(F_{required,i} - F_{actuator,i})^2} \tag{4.31}$$

where $F_{required}$ is the required cable force, $F_{actuator}$ is the simulated actuator force, and the sum is over N points where the forces are compared. In this example, there are 181 force points corresponding to $\alpha = 0°$ *to* $180°$. With $N = 181$, the RMS value is 172.4.

One method to reduce the errors between the required force and actuator force is to change the cable length between the shoulder pulley and pulley 3. This will shift the actuator output forces so that they begin and end at with an offset in the angle α. When the cable length is reduced $l = \frac{20° \times 2 \times \pi \times r_3}{360°} = 8.73mm$, the graph of the actuator output is shifted 20° to the left (towards smaller values of α). Specifically, this corresponds to pulley 2 being already rotated $\alpha = 20°$ and there being a small cable force when the arm is oriented vertically with the hand up. The new comparison between the simulated cable force and the needed cable force is shown in Figure 4.19. In this condition, the maximum cable force difference is about 220 N, which occurs when $\alpha \approx 180°$, $\theta \approx 160°$, and the calculated root mean square (RMS) is 100.3. The reduced RMS value and reduced maximum difference indicate that this method is effective in making the curves match more closely.

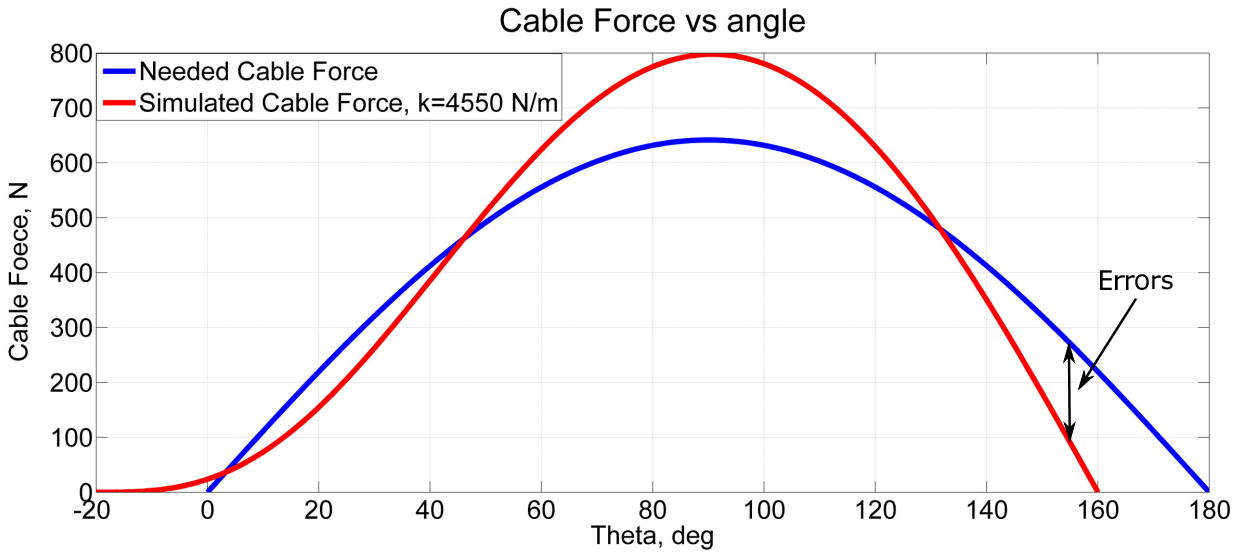

Figure 4.19: New comparison between the needed cable force and simulated cable force when reducing the cable length between the shoulder pulley and Pulley 3.

Another method to scale and shift the actuator output forces to match the needed cable force is to change the radius of pulley 3 relative to the radius of the shoulder pulley, while keeping the rest of the components unchanged. Making the radii of the shoulder pulley and pulley 3 unequal creates a gear ratio between the two pulleys. When pulley 3 rotates 180°, the shoulder pulley will rotate a larger or smaller amount depending on the gear ratio. To reduce the impact of the very low forces from the actuator output at small angles of α, it is desirable to have the shoulder pulley smaller than pulley 3. Then, the actuator output from $30° < \alpha < 180°$ can be mapped to the shoulder rotation angle θ from 0° to 180°. This can be combined with the previous method of changing the cable length between pulley 3 and the shoulder pulley. In general, when the arm rotates θ, pulley 3 rotates through an angle $\alpha = \frac{r_{sp}}{r_3}\theta$.

For example, when the radius of the shoulder pulley is decreased from 25 mm to 19.5 mm, and there is an additional shift of 50.77 degrees, this results in torque around the shoulder pulley shown in Figure 4.20. This simulation used $k = 4680$ N/m so that the peak torque from the actuator output matched the required torque. In this simulation, the scaling and

shift of the output maps the original actuator output between $\alpha = 39.6°$ and $\alpha = 180°$ to the shoulder angle $\theta = 0°$ to $\theta = 180°$. With this scaling and shift, the actuator output matches the required shoulder torque with a maximum difference of 3 $N \cdot m$ at 0 degrees, and an RMS difference of 0.72.

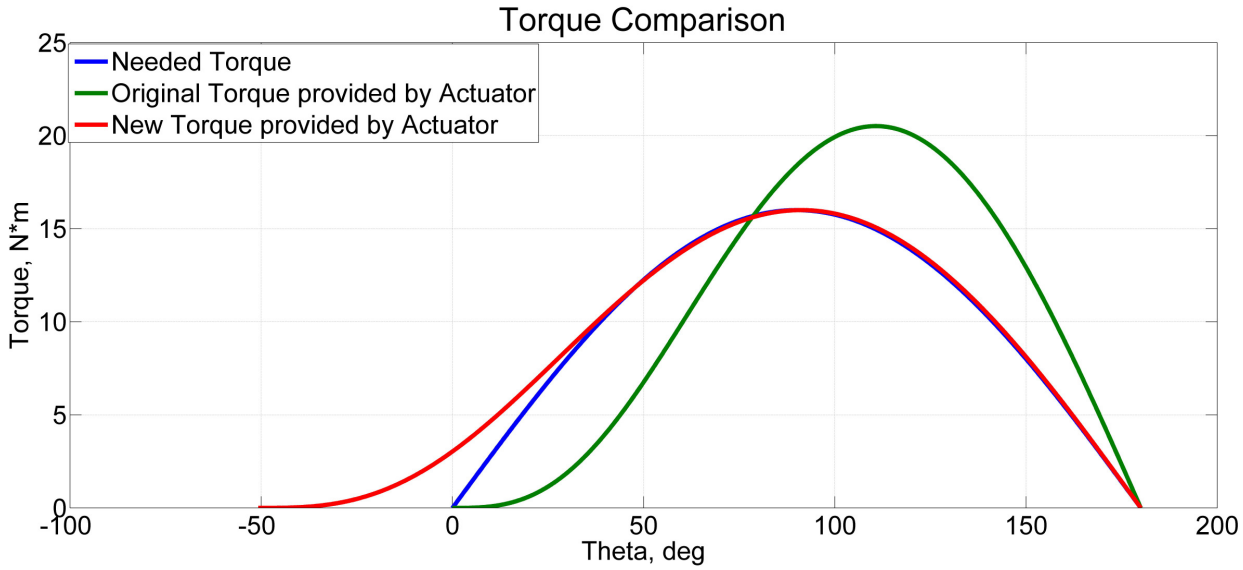

Figure 4.20: New comparison between required torque at the shoulder and the new simulated torque from the cable when changing the size of the shoulder pulley to $r_{sp} = 19.5mm$, while the actuator pulley 3 remains $r_3 = 25mm$, and a cable length reduction to correspond to a shift of 50.77 degrees.

In this section we have discussed methods of getting the actuator output force to align more closely with that required to lift the arm. However, it is important to understand the behavior of the basic actuator structure. As such, the rest of this thesis will deal with sizing and testing the original structure.

4.3.9 Pulley Dimension Selection

Following the determination of the basic dimensions of the pulley and rubber structure, the thicknesses of all pulleys are still unknown and specific values will be discussed next. While a pulley could be made to be any thickness with other fabrication methods, analyzing

the thickness in terms of multiples of 1/4" leads to a more intuitive understanding. Additionally, the elastic belts are practically available only in multiples of 1/16" so it makes sense to analyze their thickness in terms of multiples of this number. Among them, the number of layers of acetal plastic will directly influence the actuator size and weight while the number of stacked rubber belts more depend on the material property. Thus, in this chapter, only the stack number of pulleys will be discussed.

In the following analysis, variable m was used to represent the number of 1/4" pulleys stacked to form the final pulley thickness, and n represents the layers of 1/16" elastic belts stacked to form the final rubber belt. The rubber belt attaches to pulley 1 and pulley 2 during the rotation, which implies the belt width should ideally match the dimensions of pulleys.

Next, the thickness will be discussed from the rubber belt standpoint. In the initial condition when $\alpha = 0°$, the total length of belt is $L_b(\alpha = 0°) = d \times \pi + 2 \times (D - L_0) = 408.76mm$. When pulley 2 rotates 180°, the total stretched length is $4L_0 = 120$ mm. Thus, the biggest strain during the work process is $strain = 4L_0/l = 29.36\%$.

$$L_{b0}(\alpha = 0°) = l = d \times \pi + 2(D - L_0) = 408.76mm \tag{4.32}$$

$$A = \frac{Fe \times L_{b0}}{E \times \Delta L_b} = \frac{k_0 \times L_{b0}}{E}, \quad A = b \times h \tag{4.33}$$

$$b = 6.35 \times m \tag{4.34}$$

$$h = 1.5875 \times n \tag{4.35}$$

$$k_0 = \frac{F_e}{\Delta L_b}\ N/m \tag{4.36}$$

where

Fe is the desired elastic force of the belt to balance the cable force

E is the Young's modulus

σ is the tensile strength

ε is the extensional strain

F is the elastic force on rubber belt under tension

A is the actual cross-sectional area through which the force is applied

ΔL_b is the amount by which the length of the belt changes

L_b is the total length of the belt

l is the original length of rubber belt

m is the number of thinner piece of pulley

n is the number of thinner layer of rubber

b is the width of the belt's cross-section

h is the height of the belt's cross-section

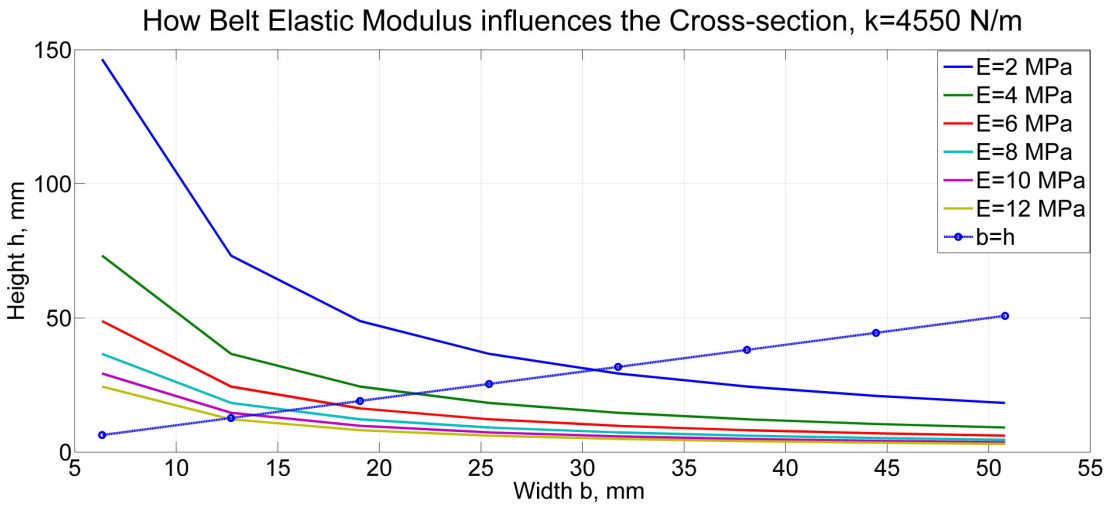

Figure 4.21: How Elastic Modulus Influences the Cross-section Area, d=76 mm L0=30mm

Young's modulus E can be calculated by dividing the tensile stress σ by the extensional strain ε. Once the rubber belts are chosen, the elastic modulus is fixed. As the initial belt length $l = 408.76mm$, $\triangle L_b = 2 \times L_0 = 120mm$ are known, the cross-section A will be the only variable that can influence the elastic force of the belt. Thus, analysis of how the transversal surface of the belt influences the elastic force was finished in MATLAB to determine the size of pulleys and belts. Variable b is the width of the cross-section and value h is the height of the cross-section. Analytical results are shown in Figure 4.21, which indicates that as the stack number of thinner pulleys increase, the required layers of belts

decrease. However, the weight of one thin pulley is heavier than one layer of rubber. Thus, a rather good pair of b and h must below the line with blue circles as depicted in Figure 4.21, namely $h < b$. According to the analysis results, when E increases, the required A decreases. To maintain the actuator in an appropriate size and weight, it is better to have a smaller A. We choose E=12 MPa, select m=4, and the corresponding width h=6.02 mm, which indicates a good pair. Thus, $m = 4$ is picked as an appropriate quantity, and there will be four thinner pulleys stacked together with the total width of 25.4 mm. As for the layer of belts, variable (n) will be discussed in Chapter 5 along with specific polymers.

Chapter 5

Detailed Design of Actuator

In this chapter, we describe the detailed design of the gravity compensation actuator, which includes: CAD of individual components and design optimization, manufacturing process selection, and polymer selections.

5.1 Pulley Design

This section discusses the design of the frame and pulleys around which the rubber is attached. As shown in Figure 5.1, 3D models were built in SOLIDWORKS to clearly represent the design of pulley 1. Pulley 1 must be fixed inside the actuator and rotates without interfering with other parts. To keep pulley 1 rotating smoothly while working, ball bearings were embedded into either side of thinner pulleys. Also, six uniformly distributed, threaded holes were placed in each thinner pulley, with the help of threaded screws and locknuts, pulley 1 is integrated. For ease of fabrication, the design was cut out of layers of acetal plastic (Delrin) on a laser cutter, stacked, and bolted together.

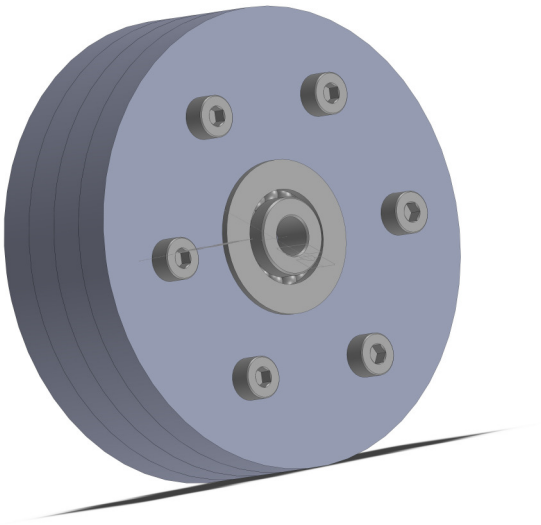

Figure 5.1: 3D Model of Pulley 1.

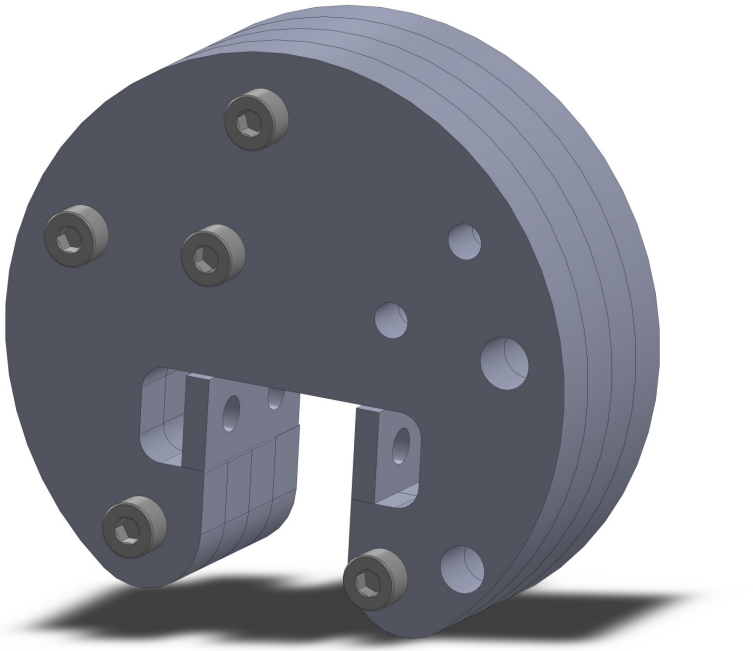

Figure 5.2: 3D Model of Pulley 2.

As mentioned above, rubber belt is attached to pulley 1 and 2; before starting to design

pulley 2, the primary problem is how to fix the belt. As depicted in Figure 5.2, a T-size groove is designed on the circle. Both belt ends will be gathered together and inserted into the groove, then squeezed and fixed by two flat clamps. The belt has to be kept in the condition that both ends touch the bottom of the T groove while the belt sides remain paralleled to the vertical inner walls of the groove. Also, it will be better to tighten the belt at the initial condition in case of sliding.

Both ends of rubber belts are punched with two holes, and two threaded screws and two locknuts are be used to fix the belt. Then, while the pulley 2 rotates, the touching areas where sharp angles exist become the most vulnerable positions, hence fillets were applied in every sharp corner to reduce abrasion and material strain. Another point is pulley 3 and pulley 2 are combined together and work as an whole, which requires same size screw holes in both pulleys. Another five screw holes were designed in pulley 2 to assemble the separate thinner pulleys.

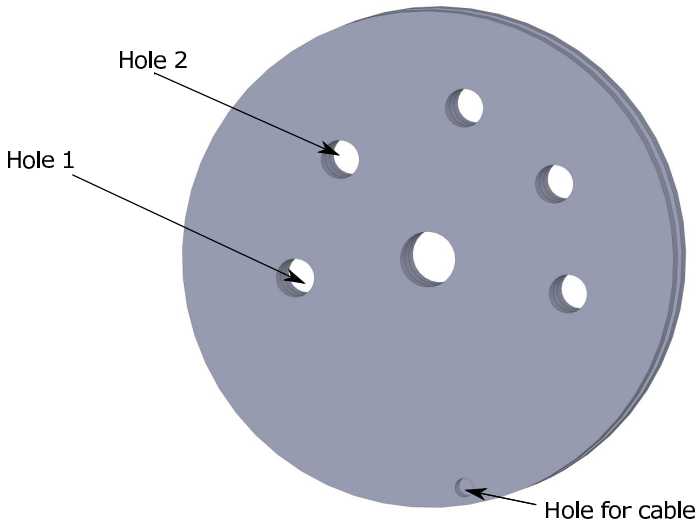

Figure 5.3: 3D Model of Pulley 3.

As shown in Figure 5.3, pulley 3 is made up of three thinner pulleys. The first one is attached to pulley 2, and acts as a wall to keep the cable on the pulley. It also includes a

hole so the cable can pass through. The middle one has the same size as the shoulder pulley with a radius of 25 mm; and the third one is almost the same as the first one except does not include cable hole. Screws through hole 1 and hole 2 connect pulley 2 and pulley 3; the remaining three holes are used to assemble pulley 3.

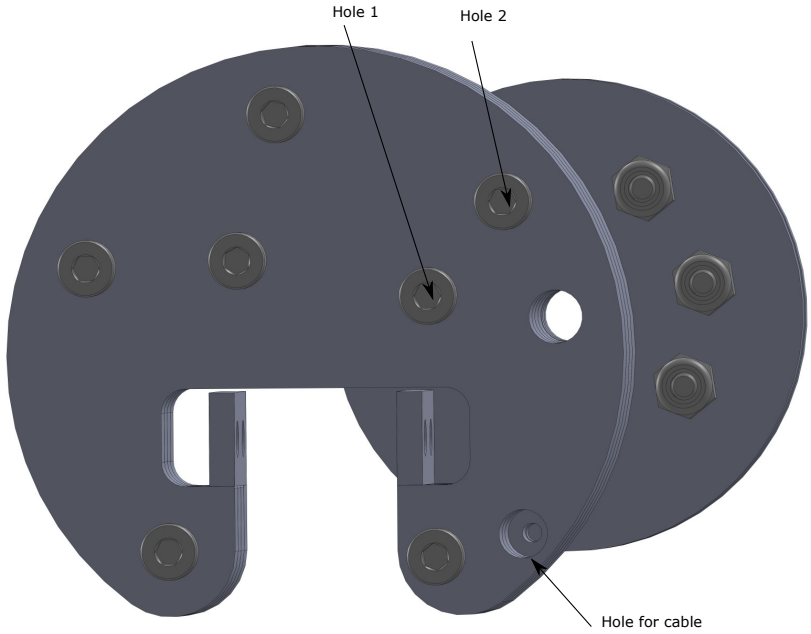

Figure 5.4: Front View of Assembly.

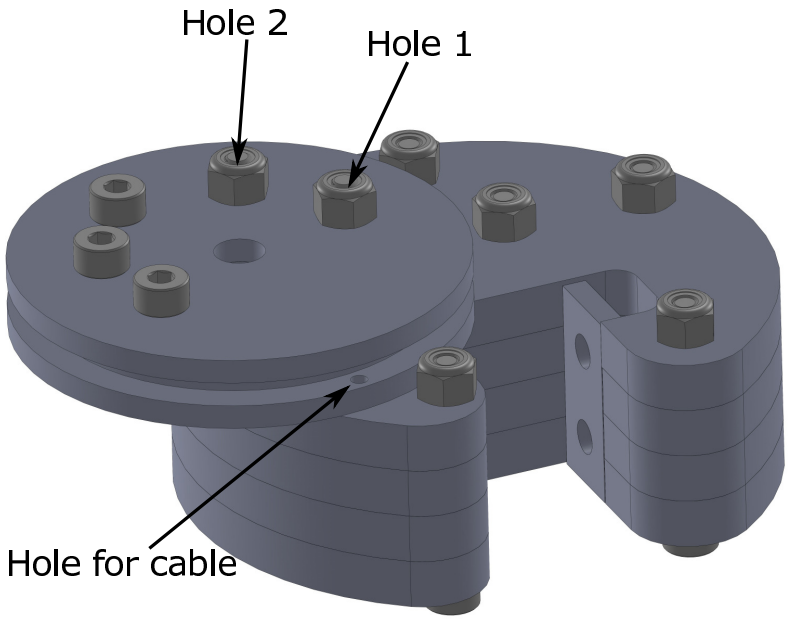

Figure 5.5: Bottom View of Assembly.

The assembly of pulley 2 and pulley 3 is shown in Figure 5.4. During the process of rotating, the rubber belt is always wrapped around pulley 2 and pulley 1 while pulley 3 connects to the shoulder pulley. Now the problem is how to balance the elastic force with the cable force. The design of cable holes can help fix it. One end of the cable is fixed by a brass stopper that is crimped onto the cable, and then inserted and placed inside the anterior side of pulley 2; the other end of the cable goes through the cable hole, wraps around pulley 3 and then comes out of the actuator from the right side of the actuator to connect the shoulder pulley. To prevent the cable from sliding, the two cable holes from the anterior side of pulley 2 must be large enough to contain the cable stopper, while the cable holes form the posterior side of pulley 2 remain the same size of the cable diameter.

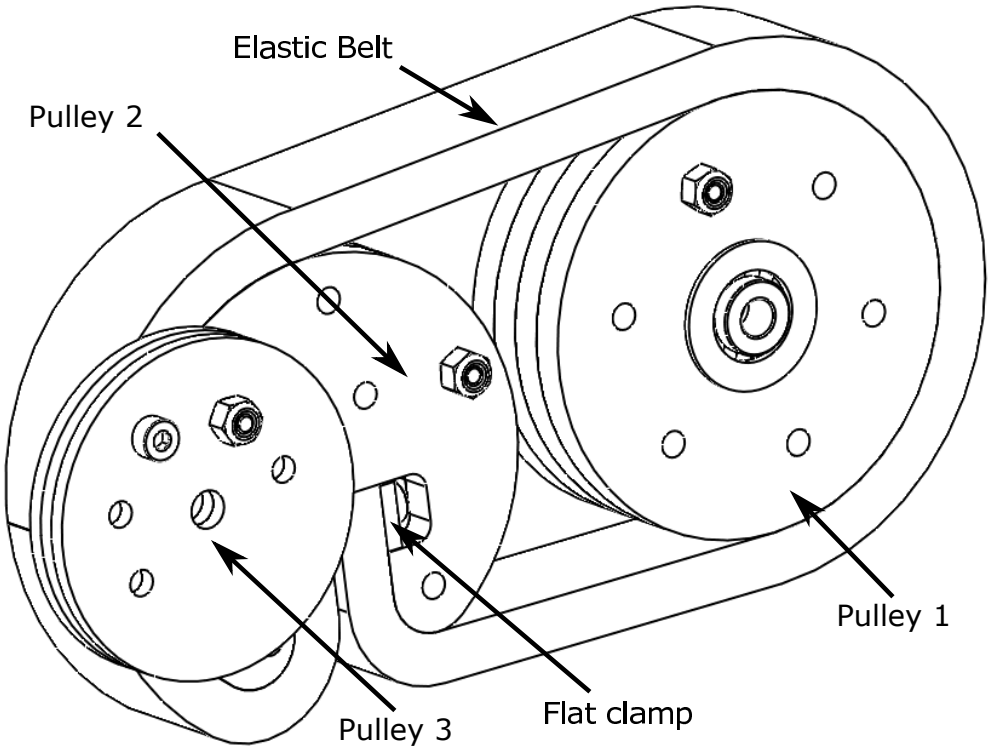

Figure 5.6: 3D model of pulley-rubber structure.

Once the design of pulleys were finished, the rubber belt can be placed in the structure. As presented in Figure 5.6, rubber belt wraps around pulley 1 and pulley 2 with two ends fixed by two screws through flat clamps. In the first place, rubber belt is tightly attached to both pulleys and along with the arm movements, rubber belt gets stretched to produce elastic force to balance the cable force.

5.1.1 Simulation of Specific Actuator

Since the specific design must clamp the rubber belt, it has a pulley that is not perfectly circular. In this section we examine how its specific shape affects the actuator's behavior.

Rotation angle, α◦	Rubber stretched length Δx, mm	Perpendicular distance L1, mm	Perpendicular distance L2, mm	Difference value L2-L1=ΔL, mm
0	0	-	-	0.00
10	1.32	31.00	37.31	6.31
20	6.96	24.50	49.11	24.61
30	12.94	18.89	56.89	38.00
40	21.79	14.41	61.59	47.18
50	31.54	11.15	64.85	53.70
60	41.85	9.08	66.92	57.84
70	52.31	8.11	67.89	59.78
80	62.61	8.12	67.88	59.76
90	72.48	8.97	67.03	58.06
100	81.69	10.55	65.45	54.90
110	90.04	12.75	63.25	50.50
120	97.38	15.46	60.54	45.08
130	103.55	18.60	57.40	38.80
140	108.46	22.08	53.92	31.84
150	109.46	25.83	50.17	24.34
160	111.80	29.21	46.22	17.01
170	112.93	32.28	42.14	9.86
180	114.00	34.88	38.00	3.12

Table 5.1: Table of Parameter Variation during Rotation Simulation in Specific Structure.

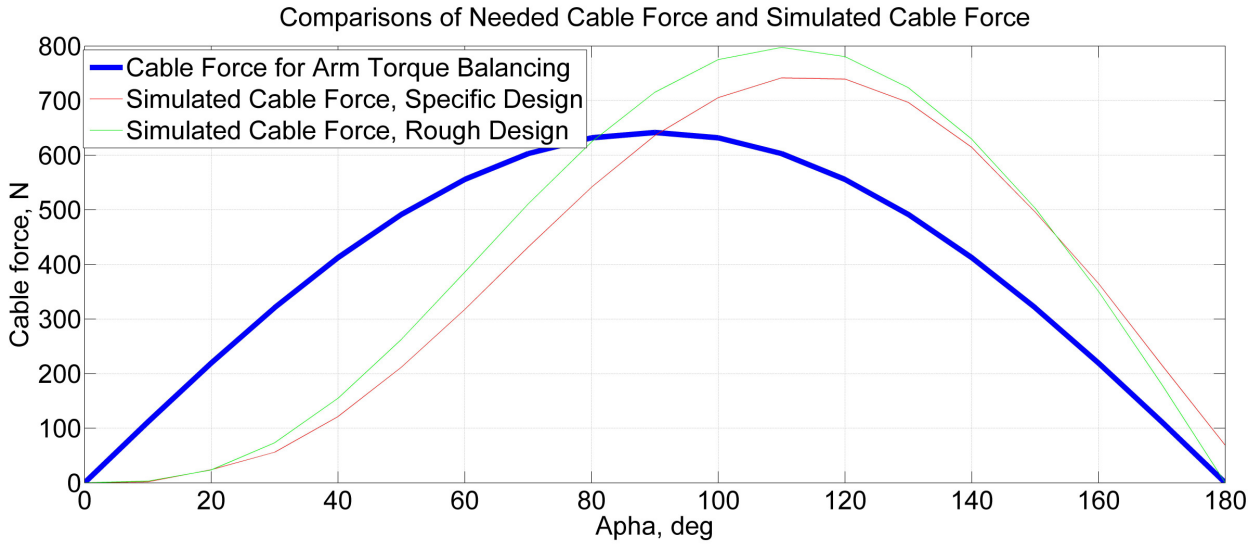

Figure 5.7: Comparison of Needed Cable Force and Simulated Cable Force, k=4550 N/m

Variations in different parameters of the specific structure are shown in Table 5.1, and comparisons between the calculated required cable force with the simulated cable force of the initial rough design and the specific design are also shown in Figure 5.7. The plot indicates that due to the shape difference of pulley 2, cable force produced by the specific design(Figure

5.6) is smaller than the rough design(Figure 4.16). The specific structure is able to provide force to hold the upper arm above the horizontal position.

5.2 Actuator Housing and Cable Connection

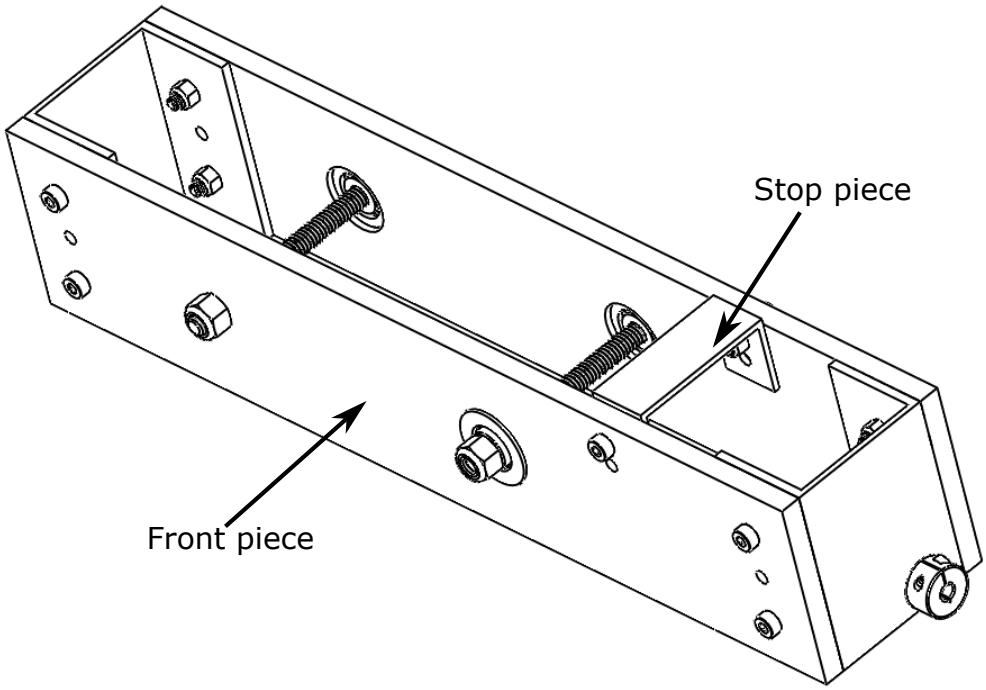

Figure 5.8: Housing of actuator.

Figure 5.8 represents the housing of the actuator, which is mainly made up of four parts: the front, back pieces and two side pieces. On one hand, ball bearings are placed inside pulley 1 to reduce the friction between pulley and the supported shaft to guarantee smooth rotation. On the other hand, to control the weight of the actuator, it is unnecessary to manufacture pulley 3 in thick materials. However, the combination of pulley 2 and pulley 3 must rotate smoothly, which requires ball bearings insert into the front and back covers. This makes the support shaft of the combination rotates together. Two side cover pieces connect with the front and back pieces by screws. The cable will come out from the right

side piece through the collar to connect the shoulder pulley.

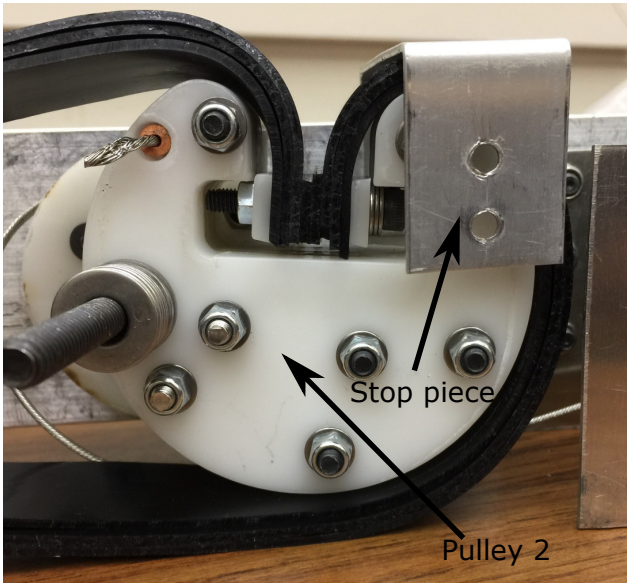

Figure 5.9: Stop piece.

After the analysis of pulley-rubber structure, elastic force will reach the peak point once α equals 180°. When pulley 2 rotates over 180°, a sudden contraction of rubber belt will occur and the elastic potential energy would rapidly decrease and disappear, which may cause safety risks. In case of such conditions, a stop piece was made and placed above the actuator. It stops pulley 2 at the extreme position and prevents rubber belt from sudden contraction.

5.3 Rubber Selection

Since all dimensions in pulley-rubber structure are determined, the next step is to select the proper polymer material. The actuator is designed for daily use in a general environment, which means there is no extra temperature requirement. During the working process, the rubber belt will be stretched repetitively to produce elastic force between two pulleys. This requires the material to be tear resistant and abrasion resistant. In addition, low cost and

easy replacement are also needed. From the McMaster-Carr website, nine kinds of polymer materials were picked and tested, as depicted in Fig(5.10) and Figure 5.11.

Figure 5.10: Polymer Samples 1-4 for Tests. Sample 1: Multipurpose Neoprene Rubber, 70A. Sample 2: Multipurpose Neoprene Rubber, 60A. Sample 3: High Temperature Silicone Rubber. Sample 4: Oil Resistant Rubber, 50A.

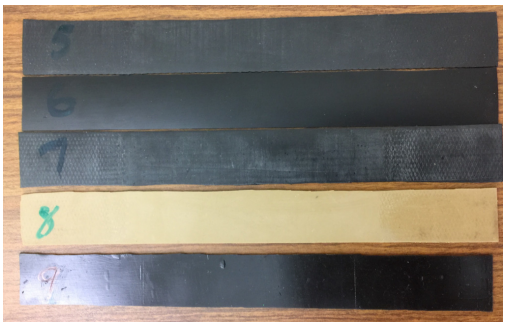

Figure 5.11: Polymer Samples 5-9 for Tests. Sample 5: Weather Resistant EPDM Rubber. Sample 6: Abrasion Resistant Polyurethane Rubber, 90A. Sample 7: Economical Abrasion Resistant SBR Rubber. Sample 8: Super Stretchable Natural Rubber. Sample 9: Abrasion Resistant Polyurethane Rubber, 60A.

5.3.1 Polymer Testing

To accurately simulate the function of the actuator and optimize the design, material property tests of the selected materials were quite important. As calculated in Chapter 4, the width of rubber belt were determined as 25.4 mm. Thus, the goal of polymer tests aimed to determine the polymer type and the thickness of actuator belt. First, 1.59 mm (1/16”) thick and 25.4 mm (1”) wide polymer samples were prepared and tested on the Instron machine

Test Samples		Max Strain=10%		Max Strain=26%		Max Strain=50%		Max Strain=100%			
Number	Materials	Energy Loss First trial (%)	Average Energy Loss , 2-5 trials (%)	Energy Loss First trial (%)	Average Energy Loss , 2-5 trials (%)	Energy Loss First trial (%)	Average Energy Loss , 2-5 trials (%)	Energy Loss First trial (%)	Average Energy Loss , 2-5 trials (%)	Elastic Modulus E (MPa)	Initial Length (mm)
1	Multipurpose Neoprene Rubber, 70A	24.17	20.26	25.90	19.16	36.78	23.30	56.53	30.59	4.17	112.65
2	Multipurpose Neoprene Rubber, 60A	23.50	18.41	24.33	17.76	26.29	18.22	37.50	21.23	2.58	109.73
3	High-Temperature Silicone Rubber	20.23	14.02	24.52	13.82	27.50	14.51	39.51	16.35	1.82	111.70
4	Oil-Resistant Buna-N Rubber, 50A	34.37	29.45	30.21	23.93	27.74	22.55	34.09	21.07	2.33	114.00
5	Weather-Resistant EPDM Rubber	27.97	19.66	35.17	24.07	43.86	31.07	60.41	42.02	4.08	113.00
6	Abrasion-Resistant Polyurethane Rubber, 90A	17.97	9.90	27.21	13.25	31.89	16.16	40.83	20.01	16.57	113.60
7	Economical Abrasion-Resistant SBR Rubber	53.92	43.77	52.59	41.98	51.92	40.81	57.58	41.26	5.48	113.60
8	Super-Stretchable Natural Rubber	5.56	3.47	6.06	4.66	6.40	3.52	10.24	3.96	1.04	115.00
9	Abrasion-Resistant Polyurethane Rubber, 60A	6.29	2.99	6.58	3.52	7.54	3.39	10.06	3.71	2.43	110.95

Table 5.2: Table of Tested Polymers.

4204 from MTS with a 1 kN load cell. Both ends of the sample belt were clutched and fully inserted into the grips, and left a length of 110 to 120 mm in between. Each sample belt was tested four times to the strains of 10%, 26%, 50%, 100% at a speed of 70 mm/min. Five repeated hysteresis trials were done in each test and there were 20 trials in total. Once all sample belts were stretched to the maximum strain, they were returned to the initial position with the same speed. All the data were collected and stored in computer, and all sample belts were tested with the same process. Details about each polymer are shown in Table 5.2.

As listed in the table, elastic modulus E and the belt energy loss percentage are the two indexes to determine the optimal material for the belt, because the energy loss percentage represents the stretch efficiency of the sample belt and the elastic modulus E has a big influence on the belt's size. Since different polymers have similar tests results, polymer 6, namely 90A abrasion-resistant polyurethane rubber, is selected to demonstrate the analysis process. As depicted in Figure 5.12a, each trial of polymer 6 is included in this strain and stress plot, the black lines represent the five hysteresis trials within the strain from 0 to 26%. For most polymers in the test, the first trial in each test is somewhat separated from the remaining four trials. Thus, the calculations about elastic modulus E were using the data from the last four trials in each test through the Equation 5.1 and choosing the average value. All the data for the calculations are shown in Figure 5.12b. The test results for the other polymers are all shown in Figures 5.13 and 5.14.

$\overline{F}$ indicates the average value of the biggest elastic force of trial 2 to 5, and $\overline{\triangle x}$ indicates the corresponding average value of increased sample length of trial 2 to 5. (l) is the initial length of the sample belt, and A is the cross-section of the sample belt. For polymer 6, in the second test where the maximum strain=26%,

$$E = \frac{F \times l}{A \times \triangle x} = \frac{k \times l}{A} \tag{5.1}$$

$$E_6 = \frac{\sigma}{\varepsilon} = \frac{\overline{F} \times l}{A \times \overline{\triangle x}} = 16.56\ MPa \tag{5.2}$$

The calculations about energy loss percentage were using Equation 5.3 for each trial. In Figure 5.12c, A_1 indicted the area filled with diagonal lines, A_2 indicted the area filled with grids. The calculated results about the last four trials were quite close, and the analysis results were also included in Table 5.2. Polymer 6, in the second test that the maximum strain=26%,

$$First\ trial,\ p_6(1) = (1 - \frac{A_2}{A_1}) \times 100\% = 27.2\% \tag{5.3}$$

$$Second\ trial,\ p_6(2) = (1 - \frac{A_2}{A_1}) \times 100\% = 13.9\% \tag{5.4}$$

$$Third\ trial,\ p_6(3) = (1 - \frac{A_2}{A_1}) \times 100\% = 13.1\% \tag{5.5}$$

$$Fourth\ trial,\ p_6(4) = (1 - \frac{A_2}{A_1}) \times 100\% = 13.1\% \tag{5.6}$$

$$Fifth\ trial,\ p_6(5) = (1 - \frac{A_2}{A_1}) \times 100\% = 12.9\% \tag{5.7}$$

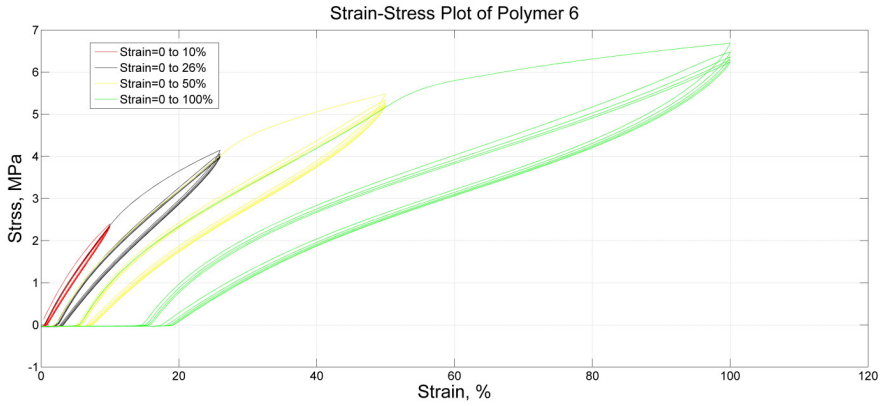

(a) Strain & Stress Plot of Polymer 6

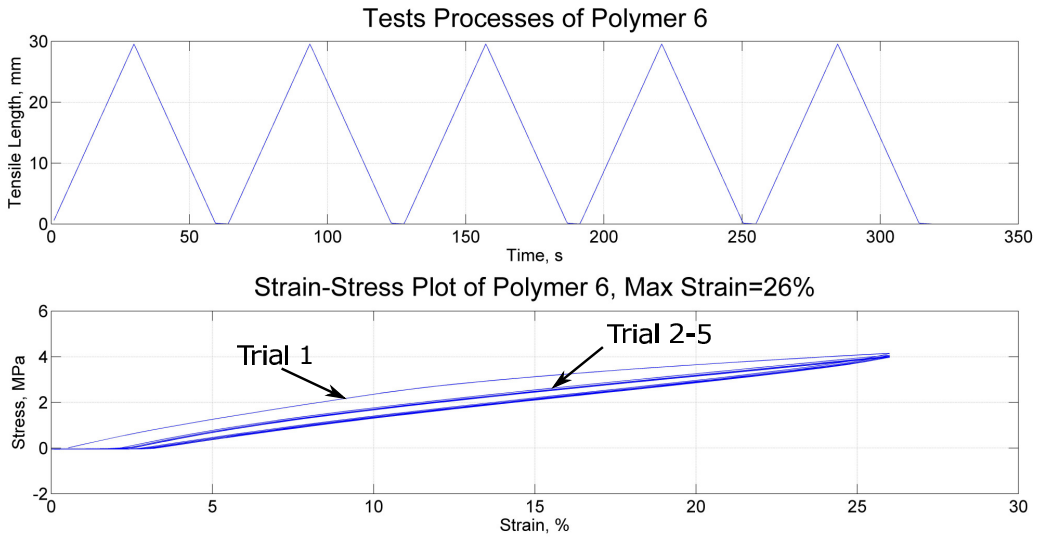

(b) Tests Results of Polymer 6 With The Maximum Strain=26%

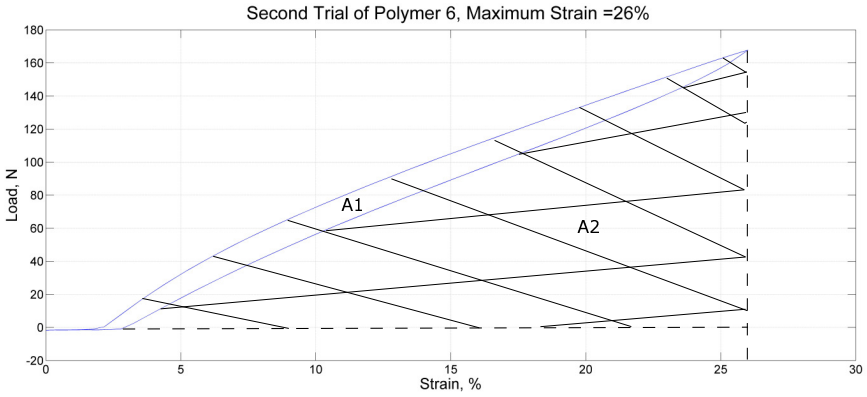

(c) Test Results of the Second Trial With The Maximum Strain=26%

Figure 5.12: Test Results of Polymer 6

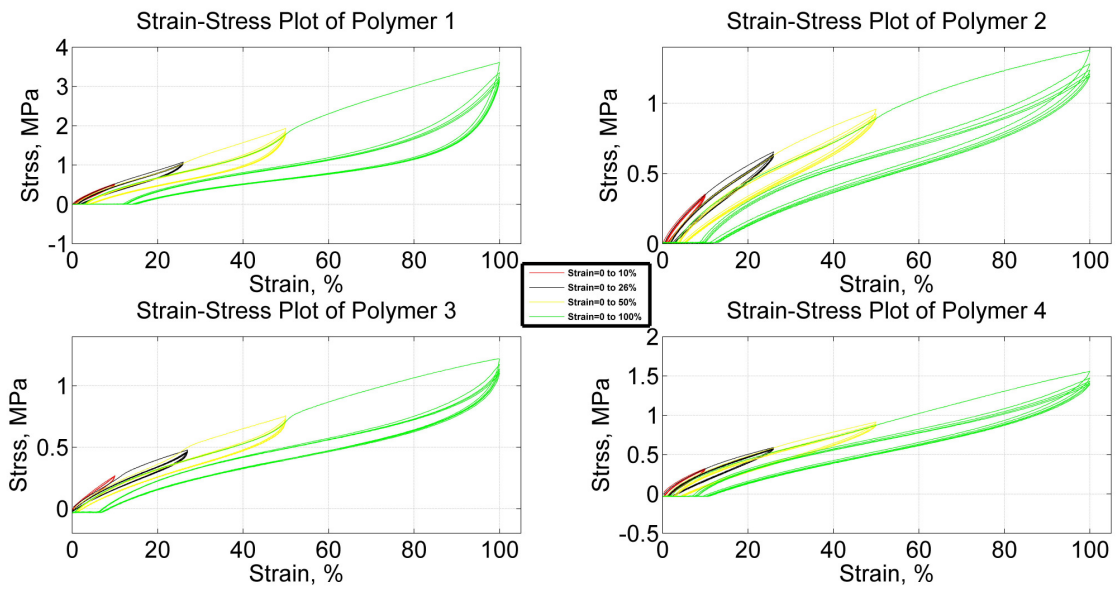

Figure 5.13: Test Results of Polymer 1 to 4.

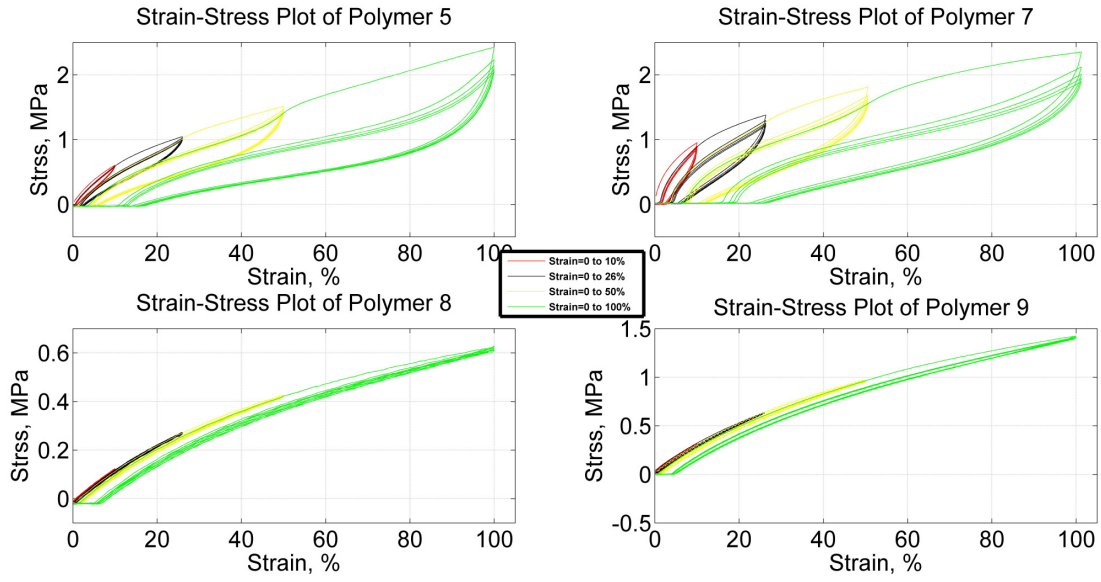

Figure 5.14: Test Results of Polymers 5,7,8,9. The sample of polymer 9 was also tested in a different test prior to this one, with different results; the former test results are included in Appendix B.2

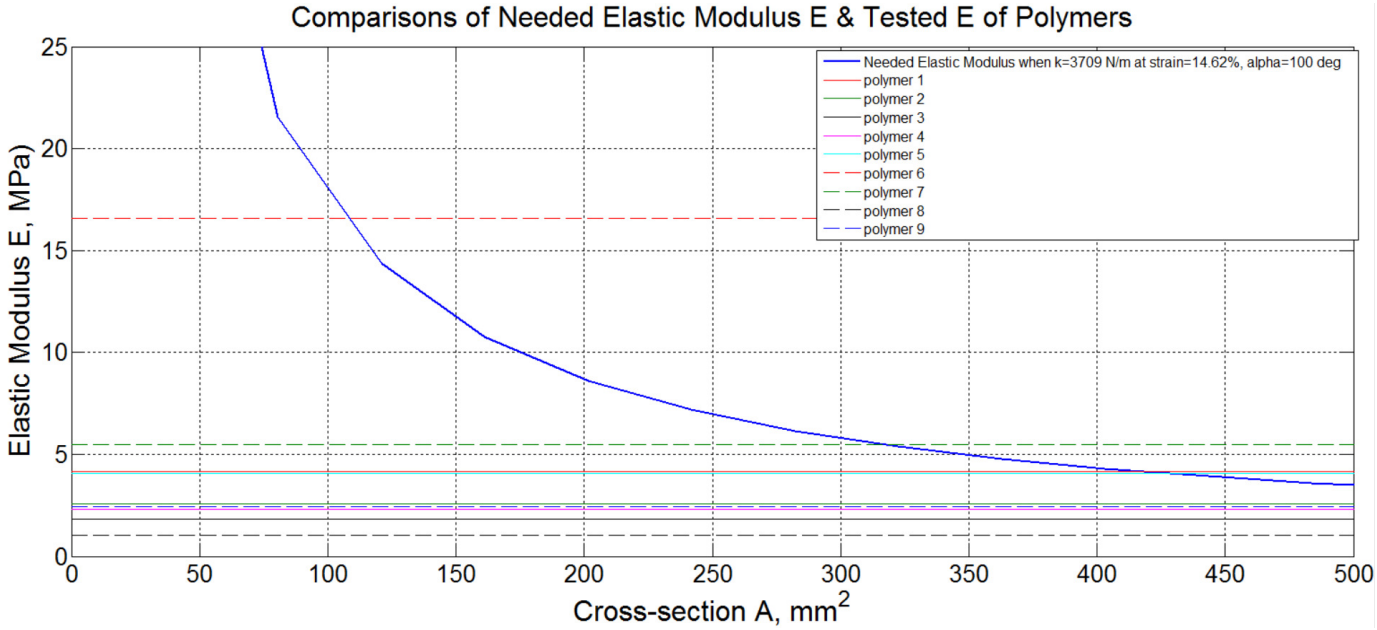

Figure 5.15: Elastic Modulus E Comparisons of Each Polymer with the Desired Value.

After computing all the elastic modulus E with the same method shown in Equation 5.1, these results were compared together to help determine the target one for the actuator. As shown in Figure 5.15, the blue curve represents the relationship between cross-section A and elastic modulus E at the position where $\alpha = 100°$. When E increases, the required A value decreases. All the computed E of tested samples were also plotted in the figure, and the comparisons indicated that polymer 6, namely 90A abrasion-resistant polyurethane rubber, is the optimal one among all the samples. While this plot aids in selecting E, there must be more analyses to help determine the belt dimensions. Even so, there is no doubt that polymer 6 is the best choice in terms of belt category.

Thus, simulations about how polymer 6 will influence the performance of the actuator were completed. This is important because the polymer has a nonlinear k value, which affects the resulting force-versus-angle curve. We simulated the actuator with the nonlinear elastomer force measured with the Instron machine, instead of using a constant k value in previous simulations in Chapter 4.3.7.

Since the maximum belt strain during the actuator movement is around 29%, the sim-

ulation was done using the polymer 6 sample belt test data at 26% maximum extension to calculate the elastic force k_s, and substituting k_s into Eq(5.11) to simulate the elastic coefficient k_a of the actuator belt. Specific k_s values used in the calculations are shown in Figure 5.16. Because polymer 6 sample belt was not fully elastic, the maximum stretch strain was close to 25% in reality. Those k_s values are varying in the stretching process. Actuator outputs are all computed using Equation 5.13.

$$l = 408.76mm,\ l_s = 110.95, \tag{5.8}$$

$$A_s = 25.4 \times 1.5875 = 39.69\ mm^2 \tag{5.9}$$

$$E = \frac{F \times l}{A \times \Delta L_b},\ k = \frac{F}{\Delta L_b} \tag{5.10}$$

$$E_6 = \frac{k_s \times l_s}{A_s} = \frac{k_a \times l}{A},\quad k_a = k_s \times \frac{l_s}{l} \times \frac{A}{A_s} \tag{5.11}$$

$$F_b = k_a \times \Delta L_b,\quad \Delta L = L_2 - L_1 \tag{5.12}$$

$$F_{output} = \frac{F_b \times \Delta L}{r_3} \tag{5.13}$$

where

F_{output} is the simulated actuator output force

F_b is the elastic force of actuator belt

E_6 is the Young's modulus of polymer 6

k_s is the computed elastic coefficient by using the data from test 2, trial 2 of polymer 6

k_a is the corresponding elastic coefficient for simulation computed from k_s

l_s is the initial length of polymer 6 test sample

F is the elastic force on rubber belt under tension

A is the cross-section of the actuator belt

A_s is the cross-section of polymer 6 test sample

r_3 is the radius of pulley 3

ΔL_b is the amount by which the length of the belt changes

L_b is the total length of the actuator belt

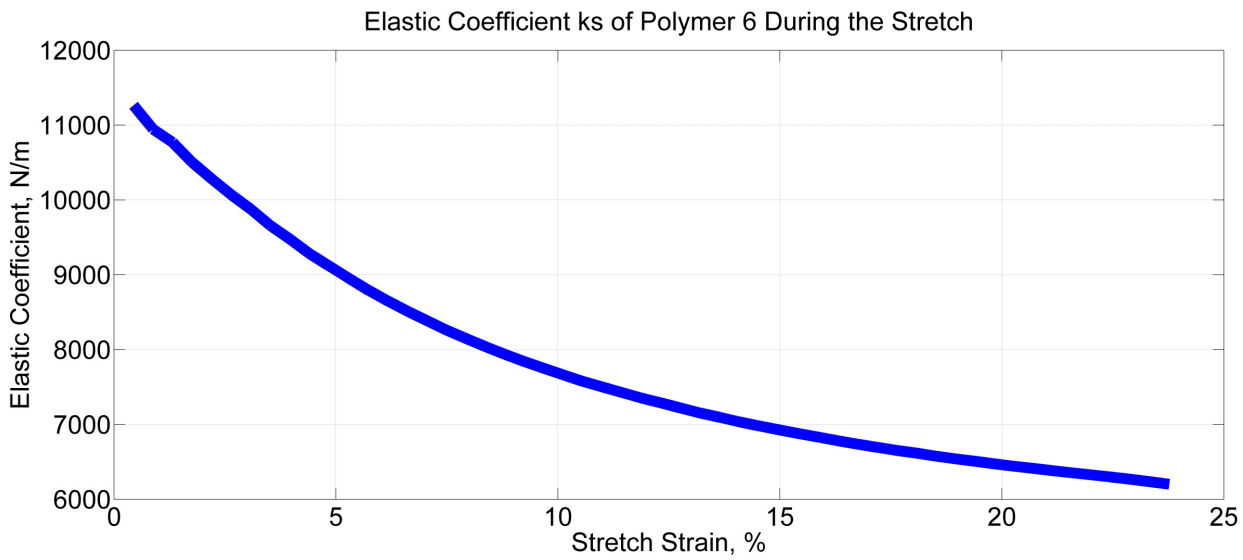

Figure 5.16: Non-linear Elastic Coefficient k_s of Polymer 6 from the Material Property Tests.

Chapter 6

Results and Discussion

To determine the efficiency of the actuator and identify improvements that can be made in the future, the performance of actuator must be tested when using the selected polymer belt, namely 90A abrasion-resistant polyurethane rubber. In this chapter, all the actuator tests aim to verify that the simulation about the passive actuator is correct, determine the optimal dimensions of the belt, and discuss how the belt will alter the way the actuator performs. Further details of the testing procedures and problems encountered during the test are included in Appendix B.

6.1 Simulation of Actuator with Polymer Tests Data

To verify the accuracy of the simulation, two tests were performed with different thicknesses of polymer 6 belts installed in the actuator. As depicted in Table 6.1, both belts have the same initial length of 408.76mm. The first belt is 25.4 mm wide and 1.588 mm thick, which corresponds to a 1/16" thick single layer of polymer 6. The second belt is 21.2 mm wide, (1.588×3) mm thick, which can be treated as two and a half layers of the first belt stacked together.

Simulations shown in Figure 6.1 are computed using Equation 5.13, and it represents the actuator output simulations in different polymer 6 belt size. For instance, the 1 layer

Polymer 6	Initial Length (mm)	Width (mm)	Thickness (mm)	Cross-section A (mm^2)
The First Belt	408.76	25.4	1.588	40.3
The Second Belt	408.76	21.2	4.76	100.9

Table 6.1: Table of Polymer 6 Belts for Actuator Tests.

simulation (red line) is used to simulate the actuator output with the first belt, and the 2.5 layer simulation (black line) is used to simulate the actuator output with the second belt.

As compared to a constant k (Figure 4.17), simulations in Figure 6.1 still have the same general shape. These simulations indicate the relationship between the actuator belt's cross-section (A) and the actuator output force. In fact, if (A) is fixed, regardless of the belt shape, the simulations about the actuator output forces are all the same.

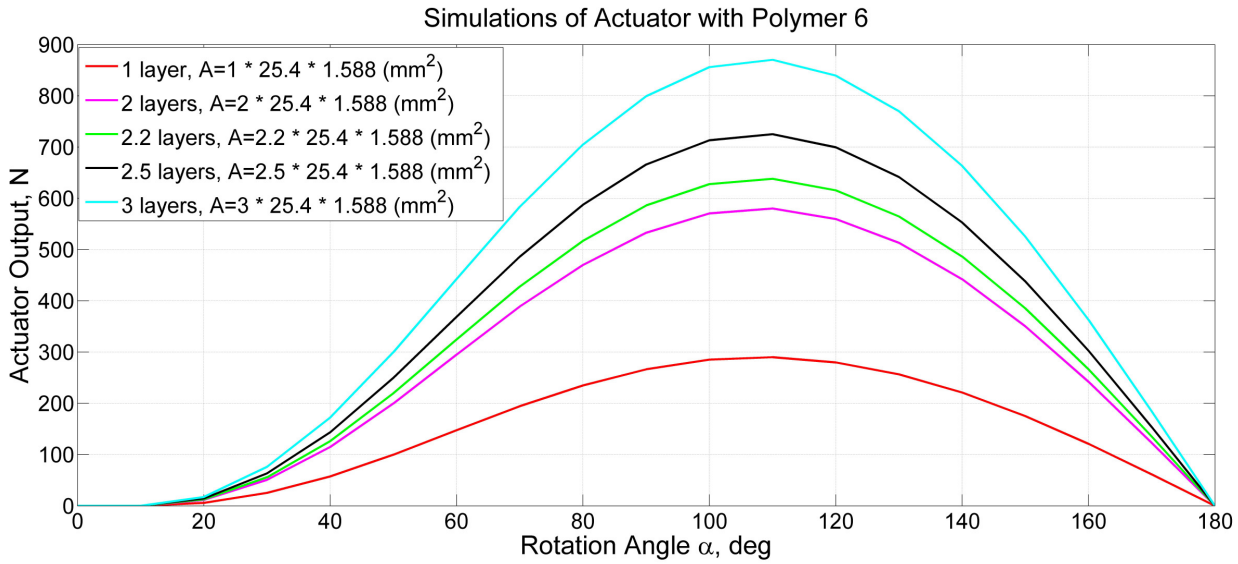

Figure 6.1: Simulation of Actuator with Polymer 6 (Rough Structure)

6.2 Test Results of Actuator

All the tests were implemented by the same Instron machine with a 1 kN load cell. The left side of the actuator was placed on the lower adapter and the wire end was fixed by the upper adapter. The whole process was controlled by a computer. The actuator was tested by the first belt and the second belt. In each case three tests were conducted, and the tests were named in test order. Among them, the first and second tests only included extending the cable, while the third test contained multiple extend-retract cycles.

6.2.1 Actuator Test Results with the First Polymer 6 Belt

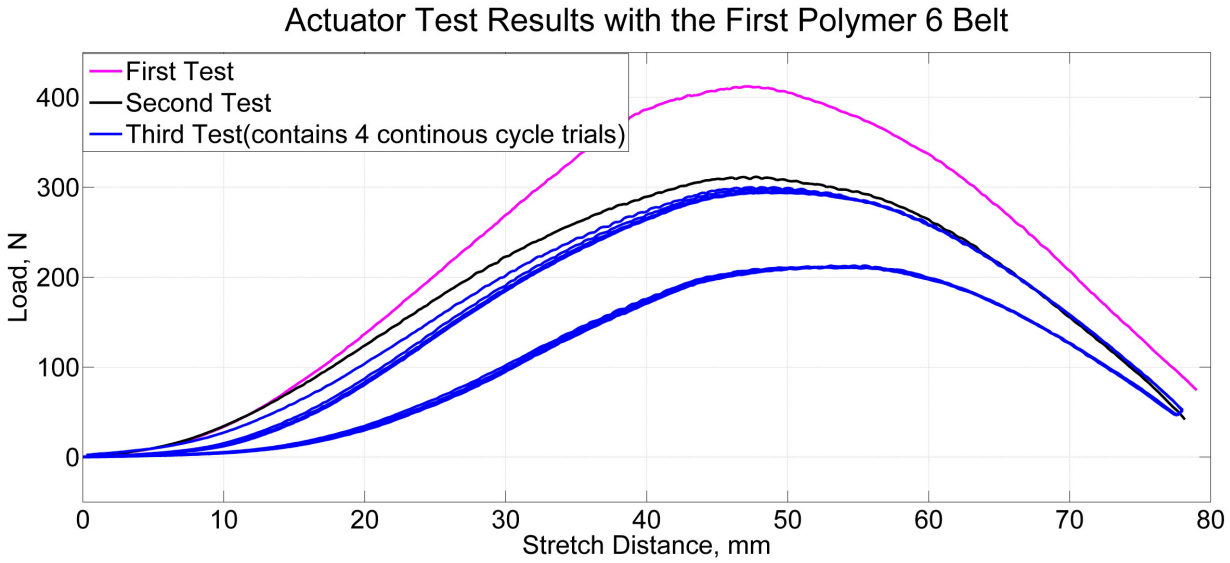

Figure 6.2: Test Results of Actuator with the First Polymer 6 Belt

Figure 6.2 indicates the tests results of actuator using the first polymer 6 belt (a single layer, 1.588 mm thick). Similar to the calculation of sample belt energy loss in Fig(5.12c), the actuator energy loss of the four cycles in the third test can be computed as

$$P = (1 - \frac{A_2}{A_1}) \times 100\% \tag{6.1}$$

where P was 35.2%, 33.5%, 33.3%, and 33.2%, respectively, for cycles 1-4.

With repetitive stretches, the energy loss of the actuator is getting closer to 33%. Comparing this value to the energy loss percentage of the polymer 6 test sample as computed in Equation 5.3, which was 13.25%, there is nearly a 20% difference between the them. This indicates that there was friction loss between different components in the actuator during its motion, such as between the belt and pulleys, and between the cable and pulleys. Likely the bulk of this loss comes from the belt rubbing against pulleys 1 and 2 as it extends and retracts.

6.2.2 Actuator Test Results with the Second Polymer 6 Belt

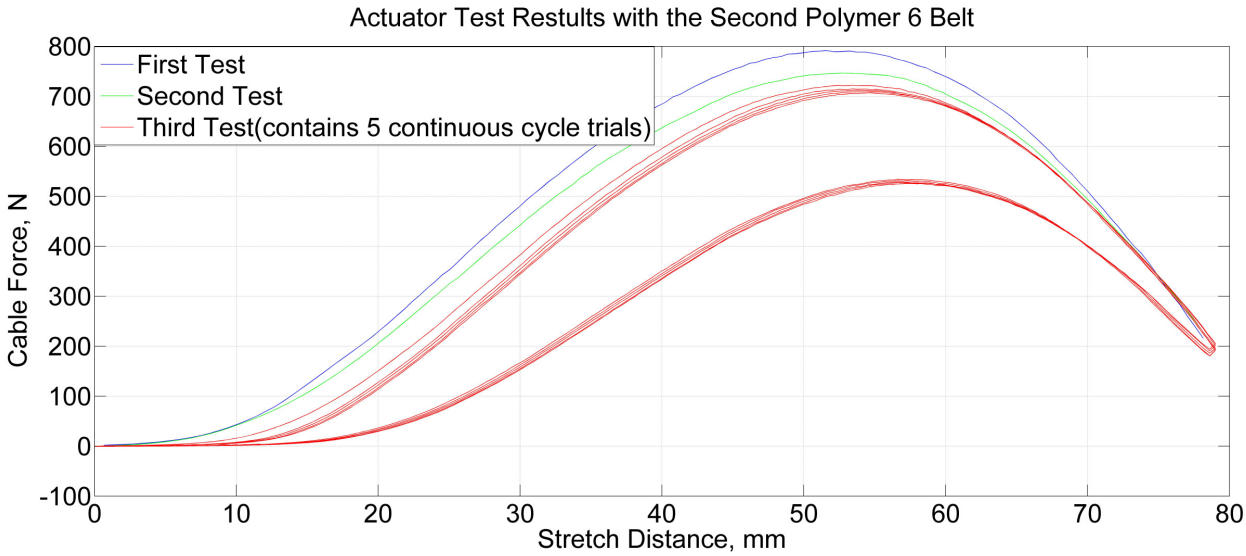

Figure 6.3: Test Results of Actuator with the Second Polymer 6 Belt

Figure 6.3 indicates the tests results of actuator installed by the second polymer 6 belt, which had a thickness of (1.588×3) mm. Using the same method to calculate the actuator energy loss of the five cycles in the third test, the test had losses of 34.1%, 32.9%, 32.7%, 32.7%, and 32.6%, respectively.

With repetitive stretches, the energy loss of the actuator with the second belt is around

33%, which is quite similar to the actuator with the first, thinner, belt. Similarly, there is a nearly 20% difference between the results of this actuator test and polymer 6 belt tests, which verifies the existence of friction loss between different components inside the actuator.

6.2.3 Actuator Test

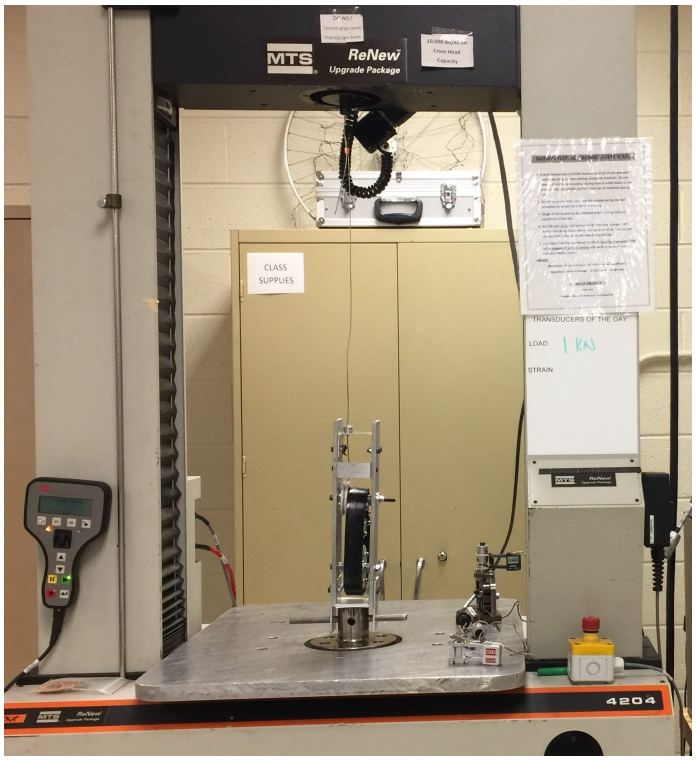

Figure 6.4: Actuator Test with Polymer 6 Belt Installed

The actuator test aimed to analyze the capability of the actuator, to measure how much force it can provide. Figure 6.4 depicts the same Instron machine after removing the wedge grips. At the lower position, connective aluminum pieces were fixed at the left end of the actuator, using a half inch rod placed through the aluminum piece and adapter. The other end was fixed by a rod, which went through a hook that was built by a cable clamp. Then, adjusting the space between the upper and lower couplings by using control panel, which was placed at the bottom left, until the detected load equaled zero. Lifting speed and return

(a) Adapter from Instron Machine

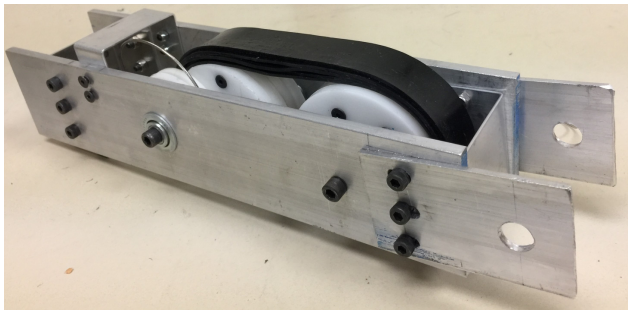

(b) Connective Aluminum Pieces Fixed on Actuator

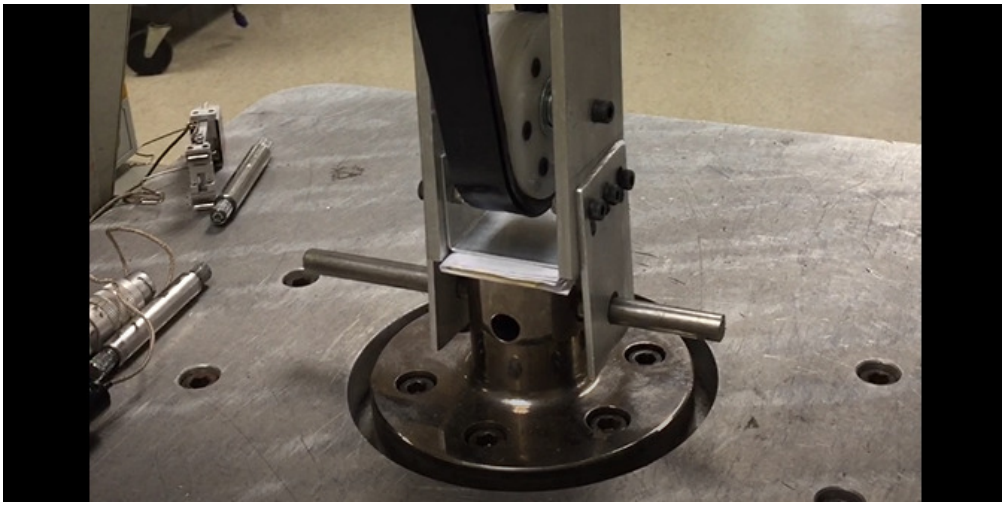

(c) Actuator is Fixed on The Adapter

Figure 6.5: How Actuator is Fixed on the Instron Machine.

speed were set the same as 65 mm/min. The maximum lifting distance was around 78 mm that enabled pulley 3 rotate 180°. When the test was finished, the load data and crosshead moving distance were collected and stored in the computer.

6.2.4 Actuator Fixturing

In addition to material test, functional testing of the actuator was also quite important. It can help determine the efficiency of the actuator and expose problems with the current design. Before doing the tests, a primary task was building a connecting structure between

the actuator and fixtures, with the purpose of maintaining the actuator in place during the testing process. According to the adapter shape (Figure 6.5a) of the Instron machine, connective aluminum pieces were designed to combine the lower base and the actuator(Figure 6.5b). With slots in either piece, the distance between the actuator and adapter can be adjusted. The left side of the actuator was placed vertically on the lower adapter, the actuator was tightly fixed with a half inch rod placed through the horizontal hole inside the adapter, as shown in Figure 6.5c.

6.3 Discussion

Due to the pulley 2 and 3 mechanism as shown in Figure 4.7, when the pulley combination rotates 180° the actuator belt will be stretched and increase 120 mm while the wire end will be pulled out with the length of $r_3 \times \pi = 78.54\ mm$, namely half circumference of pulley 3. Thus, transferring the experimental data of the pulled out wire end distance (l_{arc}) into the corresponding rotation angle α by using Equation 6.2, the comparisons between the test results and the simulation are depicted in Figure 6.6.

$$\alpha = \frac{l_{arc} \times 360^\circ}{\pi \times 2 \times r_3} \tag{6.2}$$

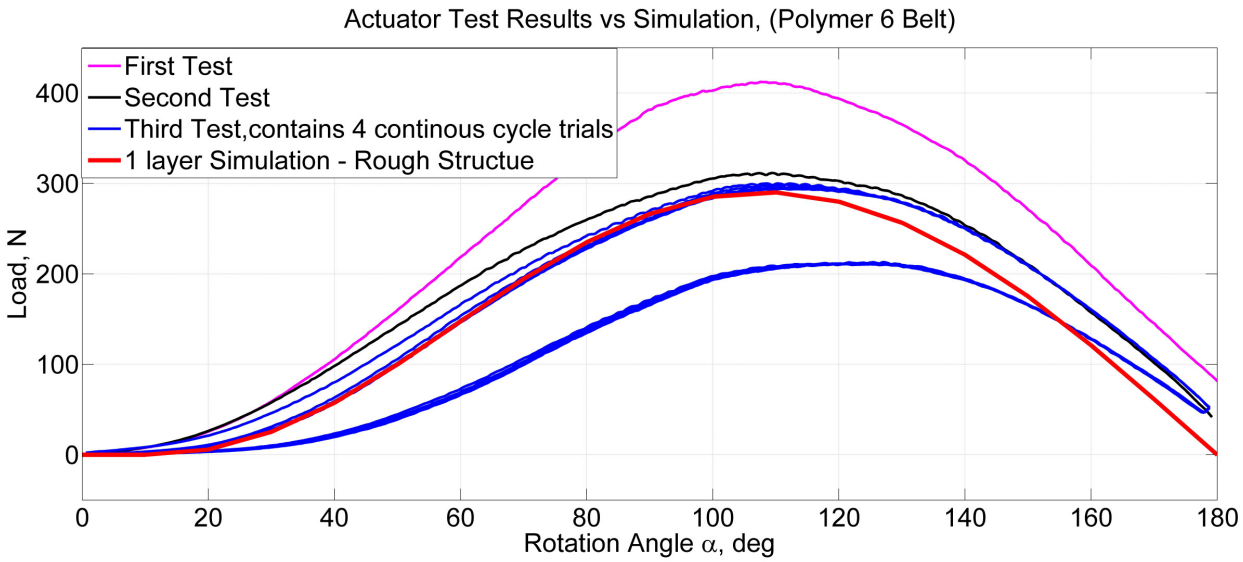

Figure 6.6: Comparison of Test Results(first belt) and Simulation(1 layer)

For the actuator with the first polymer 6 belt, the comparisons between simulations and actuator test results are shown in Figure 6.6, which imply that when the actuator is repetitively stretched, the outputs are getting closer to the simulated actuator output forces. The simulation is from Figure 6.1. This also verifies the simulation method is quite reliable.

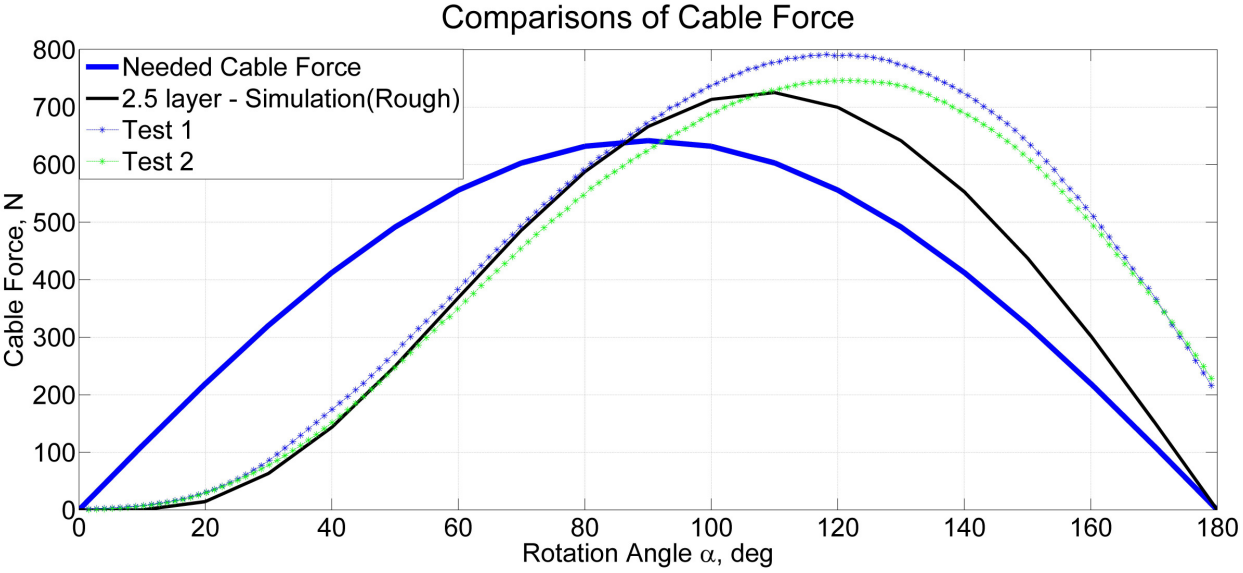

Figure 6.7: Comparison of the First Two Test Results(second belt) and Simulation(2.5 layers)

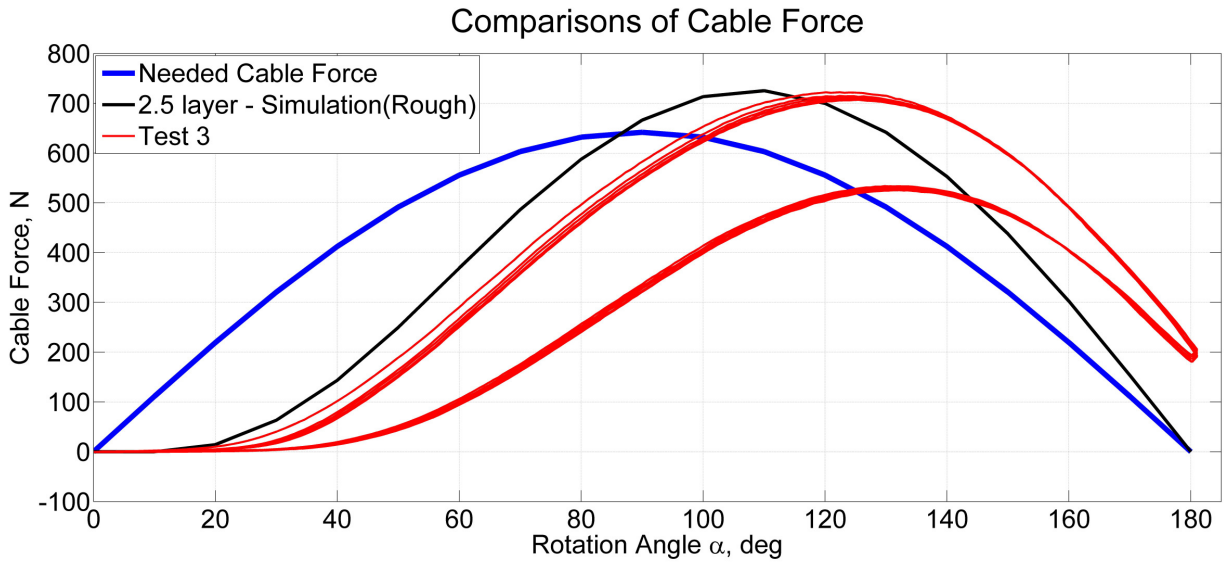

Figure 6.8: Comparison of the Third Test Results(second belt) and Simulation(2.5 layers)

For the tests with the second (thicker) polymer 6 belt, comparisons between the 2.5 layers simulation and actuator test results are shown in Figures 6.7 and 6.8, which indicate that when the actuator is repetitively stretched, the shape of the outputs is getting closer to the simulated actuator output forces. The simulation is from Figure 6.1. Different from the former comparison(Figure 6.6), there is an angle shift about 10° between the simulation and test results. This is because the actuator belt was slightly loose, such that it was not tightened at the beginning when $\alpha = 0°$ until $\alpha > 10°$. The similar cable force shape between the simulation and actuator test results can also verify the reliability of simulation method.

The next step is to determine an optimal dimension for actuator belt that enables the actuator to support the arm around the horizontal position. When using the current pulley-rubber structure (Figure 5.6), according to the simulations shown in Figure 6.9: when using 2.2 layers of the polymer 6 belt (cross-section $A = 2.2 \times 1.5875 \times 25.4 = 88.8\ (mm^2)$), the actuator is able to balance the arm around $\theta = 100°$; when using 2.5 layers of the polymer 6 belt (cross-section $A = 2.5 \times 1.5875 \times 25.4 = 100.8\ (mm^2)$), the actuator is able to balance the arm around $\theta = 85°$; and when using 3 layers of the polymer 6 belt (cross-section $A = 3 \times 1.5875 \times 25.4 = 121\ (mm^2)$), the actuator is able to balance the arm around $\theta = 70°$.

Therefore, selecting cross-section value (A) in the range of 88.8 (mm^2) *to* 100.8 (mm^2) for the actuator belt will be a good option so that the actuator is able to balance the arm in the horizontal position. An offset can be included between the pulley 3 in the actuator and a pulley located at the shoulder of an arm exoskeleton, thereby allowing the force versus angle curve to shift to the left or right. This will allow the peak of the desired force to occur at the same angle as the peak of the actuator force.

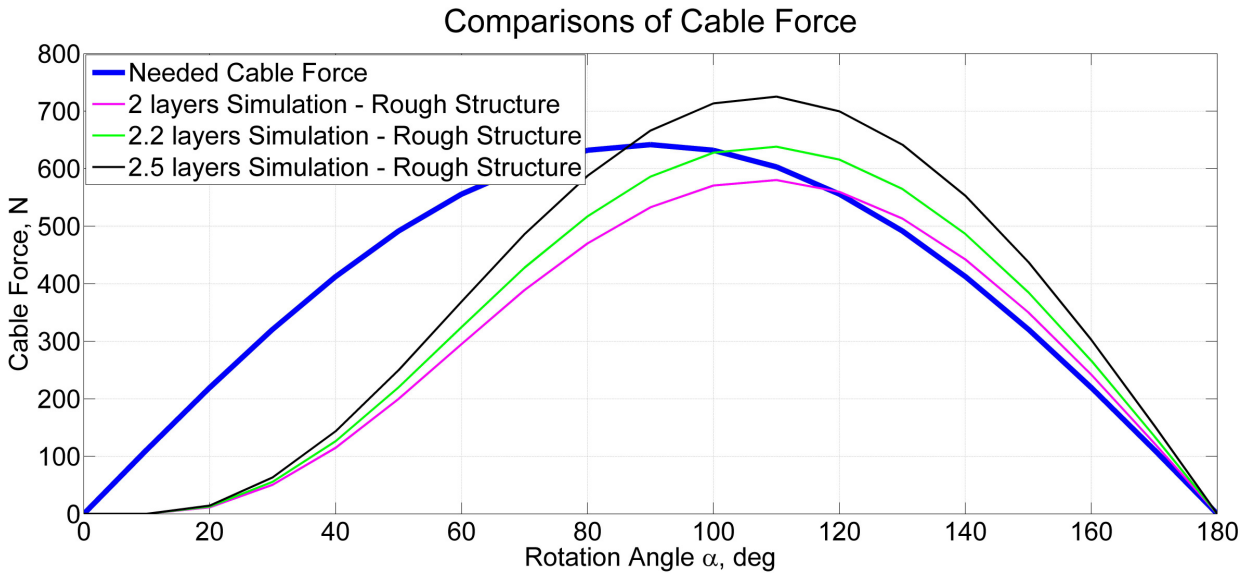

Figure 6.9: Comparisons of Simulations and Needed Cable Force

Chapter 7

Conclusion

A small, portable passive actuator was proposed for assistance of human upper extremity to reduce the risk of repetitive strain injury and improve work efficiency. The maximum force that the actuator can provide depends on the belt's material and dimensions. According to the actuator tests, when the actuator uses a 90A abrasion-resistant polyurethane rubber belt with the dimensions of initial length of 408.76 mm and cross-section (A) is $40.3mm^2$, the maximum force that the actuator can produce is near 300 N when pulley 2 rotates 110°. At this maximum output position, if the actuator is connected to a shoulder joint and an arm exoskeleton, it can supply force to support approximately 50% of the arm's weight. If the actuator uses the same rubber belt with an initial length of 408.76 mm and a cross-section (A) of $100.9mm^2$, the maximum force that the actuator can produce is near 720 N in extension and 530N in retraction, which are roughly 112% and 83% of the torque required to lift a human arm, respectively. The whole device can be easily constructed and maintained.

The pulley-rubber structure is the main body of the actuator with the function of producing elastic force and connecting with other external devices. If the actuator is used with a flexible shoulder joint and an arm exoskeleton, gravity compensation will be produced on the upper extremity in conjunction with the arm movements.

7.1 Recommendations

The components of the actuator can be divided into two types, those manufactured and those purchased. Most of the purchased parts came from the website McMaster-Carr (www.mcmaster.com). The purchased polymer materials are responsible for much of the hysteresis in the actuator. However, the manufactured parts were built by different hand-operated mechanical processes, and the manual manufacturing errors may affect the quality of the assembly. All the pulleys were combined by different pieces that were manufactured by laser cutting machine with accurate dimensions. But to assemble the different laser cut pieces together, screws were used which may cause varying tolerances. Thus, it would be better to manufacture each pulley as a whole with a CNC milling machine.

Additionally, the pulley-rubber structure was supported by an aluminum cover. Rather thick pieces were selected to conservatively prevent actuator disintegration. The current actuator is about 1.6 kg which is not light enough for wearable structures. Therefore, finite element analysis is necessary to identify how light the structure can be made.

7.2 Future Work

There is still space to improve the passive actuator. The original goal of the actuator was to assist the workers in industry who are facing the risk of occupational injuries due to repetitive heavy work. An ideal actuator must be able to provide enough energy to upper extremity with any arm movements at any time. According to the actuator tests in Chapter 6, only simulations using polymer 6 material were verified. The corresponding inferred optimized range of cross-section (A) is between 88.8 to 100.8 mm^2. Thus, the next step is to look for other strong polymer materials that have properties comparable to those of polymer 6. In addition, workers work for long hours everyday, it requires the actuator must be light and small enough that it will not lead to exhaustion. Therefore, a reduction of the actuator size and an optimization with respect to weight are important. Also, to make the current actuator output forces perfectly match the needed cable force to balance the weight

of human arm, the shape of the combination of pulley 2 and pulley 3 could be redesigned. The new created cam element would have an appropriate contour, with a variable radius. Additionally, the cable length between the actuator and a pulley on a shoulder exoskeleton could be changed, and the diameter of the shoulder pulley could be made different than that of pulley 3. Each of these techniques could be used to make the actuator output force match the desired force profile more closely.

Since the passive actuator has been created, methods of connecting with external devices must be developed. First, a suitable vest that the actuator can properly be mounted on must be created. Also, the design of a flexible shoulder joint that is able to be mounted on the same vest must be finalized. Then, a specific design of the arm exoskeleton must be created, or the output mechanism of the actuator can be modified to work with other exist arm exoskeleton products.

Bibliography

[1] M. J. A. Jannink, A. M. M. Aalsma, and H. V. D. Kooij, "Freebal : dedicated gravity compensation for the upper extremities," vol. 00, no. c, pp. 804–808, 2007.

[2] T. Rahman, R. Ramanathan, R. Seliktar, and W. Harwin, "A simple technique to passively gravity-balance articulated mechanisms," *Journal of Mechanical Design*, vol. 117, no. 4, pp. 655–658, 1995.

[3] K. A. Wyrobek, E. H. Berger, H. M. Van der Loos, and J. K. Salisbury, "Towards a personal robotics development platform: Rationale and design of an intrinsically safe personal robot," in *Robotics and Automation, 2008. ICRA 2008. IEEE International Conference on*, pp. 2165–2170, IEEE, 2008.

[4] K. Koser, "A cam mechanism for gravity-balancing," *Mechanics Research Communications*, vol. 36, no. 4, pp. 523–530, 2009.

[5] N. Takesue, T. Ikematsu, H. Murayama, and H. Fujimoto, "Design and Prototype of Variable Gravity Compensation Mechanism (VGCM)," pp. 249–257, 2011.

[6] T. Nakayama, Y. Araki, and H. Fujimoto, "A New Gravity Compensation Mechanism for Lower Limb Rehabilitation," pp. 943–948, 2009.

[7] J. M. Muggleton, R. Allen, and P. H. Chappell, "Hand and arm injuries associated with repetitive manual work in industry : a review of disorders , risk factors and preventive measures," vol. 0139, no. August, 2017.

[8] M. V. Tulder, A. Malmivaara, and B. Koes, "Repetitive strain injury," no. 14, pp. 1815–1822, 2007.

[9] B. A. Silverstein, L. J. Fine, and T. J. Armstrong, "Hand wrist cumulative trauma disorders in industry," pp. 779–784, 1986.

[10] J. Greening, "Vibration sense in the upper limb in patients with repetitive strain injury and a group of at-risk of ® ce workers," pp. 29–34, 1998.

[11] R. Williams and M. Westmorland, "Occupational cumulative trauma disorders of the upper extremity," *American Journal of Occupational Therapy*, vol. 48, no. 5, pp. 411–420, 1994.

[12] K. Kroemer, "Cumulative trauma disorders: their recognition and ergonomics measures to avoid them," *Applied ergonomics*, vol. 20, no. 4, pp. 274–280, 1989.

[13] S. A. t. L. 3M, "StrongArm® ErgoSkeleton™ Lift Assist Device V22-L."

[14] S. A. Green, M. Billinghurst, X. Chen, and J. G. Chase, "Human-robot collaboration: A literature review and augmented reality approach in design," *International Journal of Advanced Robotic Systems*, vol. 5, no. 1, p. 1, 2008.

[15] N. Ulrich and V. Kumar, "Passive mechanical gravity compensation for robot manipulators," in *Robotics and Automation, 1991. Proceedings., 1991 IEEE International Conference on*, pp. 1536–1541, IEEE, 1991.

[16] T. Morita, F. Kuribara, and S. Sugano, "A Novel Mechanism Design for Gravity Compensation in Three Dimensional Space," pp. 163–168, 2003.

[17] S. Shirata, A. Konno, and M. Uchiyama, "Design and Evaluation of a Gravity Compensation Mechanism for a Humanoid Robot," pp. 3635–3640, 2007.

[18] rethink robotics, "Baxter."

[19] R. Robotics, "Baxter datasheet," 2016.

[20] T. Rahman, W. Sample, R. Seliktar, M. Alexander, and M. Scavina, "A body-powered functional upper limb orthosis," *Journal of rehabilitation research and development*, vol. 37, no. 6, p. 675, 2000.

[21] S. J. Ball, I. E. Brown, and S. H. Scott, "Medarm: a rehabilitation robot with 5dof at the shoulder complex," in *Advanced intelligent mechatronics, 2007 IEEE/ASME international conference on*, pp. 1–6, IEEE, 2007.

[22] M. G. van Elk, B. J. Driessen, M. Dorrepaal, J. J. van der Werff, E. G. van der Meché, and A. P. Aulbers, "A motorized gravity compensation mechanism used for active rehabilitation of upper limbs," in *Rehabilitation Robotics, 2005. ICORR 2005. 9th International Conference on*, pp. 152–155, IEEE, 2005.

[23] T. Nef, M. Mihelj, and R. Riener, "Armin: a robot for patient-cooperative arm therapy," *Medical & biological engineering & computing*, vol. 45, no. 9, pp. 887–900, 2007.

[24] T. G. Sugar, J. He, S. Member, E. J. Koeneman, J. B. Koeneman, R. Herman, H. Huang, R. S. Schultz, D. E. Herring, J. Wanberg, S. Balasubramanian, P. Swenson, and J. A. Ward, "Design and Control of RUPERT : A Device for Robotic Upper Extremity Repetitive Therapy," vol. 15, no. 3, pp. 336–346, 2007.

[25] SUITX, "shoulderX."

[26] I. Levitate Technologies, "Levitate AIRFRAME."

[27] S. K. Agrawal and A. Fattah, "Theory and design of an orthotic device for full or partial gravity-balancing of a human leg during motion," *IEEE Transactions on Neural Systems and Rehabilitation Engineering*, vol. 12, no. 2, pp. 157–165, 2004.

[28] P.-y. Lin, W.-b. Shieh, and D.-z. Chen, "A theoretical study of weight-balanced mechanisms for design of spring assistive mobile arm support (MAS)," *MAMT*, vol. 61, pp. 156–167, 2013.

[29] S. Landsberger, P. Leung, V. Vargas, J. Shaperman, J. Baumgarten, L. Yasuda, E. Sumi, D. McNeal, and R. Waters, "Mobile arm supports: history, application, and work in progress," *Topics in Spinal Cord Injury Rehabilitation*, vol. 11, no. 2, pp. 74–94, 2005.

[30] A. H. Stienen, E. E. Hekman, F. C. Van der Helm, G. B. Prange, M. J. Jannink, A. M. Aalsma, and H. Van der Kooij, "Dampace: dynamic force-coordination trainer for the upper extremities," in *Rehabilitation Robotics, 2007. ICORR 2007. IEEE 10th International Conference on*, pp. 820–826, IEEE, 2007.

[31] J. Orthopedic, "Wilmington Robotic Exoskeleton."

[32] E. BIONICS, "ekso BIONICS Arm Support."

[33] P. De Leva, "Adjustments to zatsiorsky-seluyanov's segment inertia parameters," *Journal of biomechanics*, vol. 29, no. 9, pp. 1223–1230, 1996.

Appendix A

Appendix A: Mechanism Construction Details

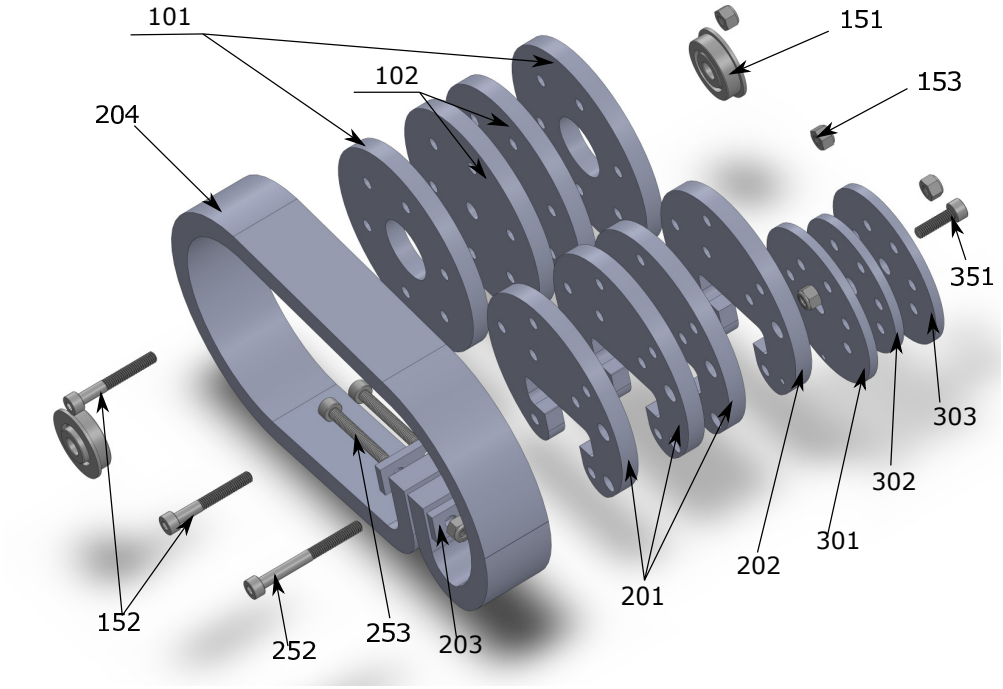

Figure A.1: Exploded View of pulley-rubber structure.

Part Number	Name of part/materials	Part description	Type
Subassembly 400- Housing of actuator			
401	Front piece	7 mm thick aluminum piece	Manufactured
402	Back piece	7 mm thick aluminum piece	
403	Left side piece	3 mm thick aluminum piece	
404	Rght side piece	3 mm thick aluminum piece	
405	Stop piece	Avoid sudden power loose	
451	Locknuts	0.25"-20	Purchased
452	Shaft	Diameter=0.25"	
453	Shaft collar	For 0.25" shaft	
454	Set screws-5	Connect front, back and side walls, M4 X 18 mm	
455	Set screws-6	Fix stop piece, M4 X 12 mmm	
151	Ball bearing	For diameter=0.25" shaft	
153	Locknuts	M4	

Table A.1: Table of actuator housing.

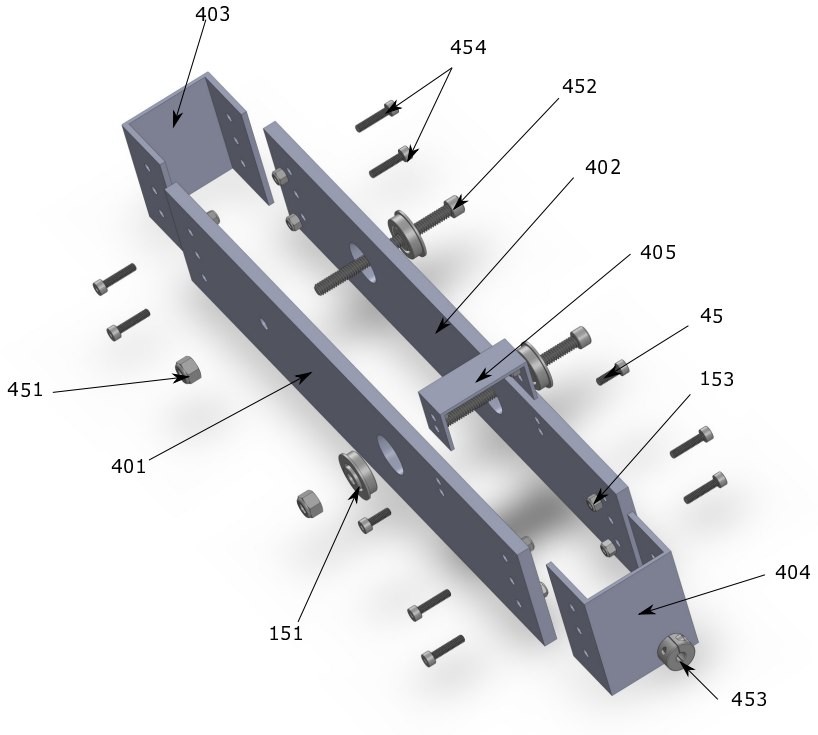

Figure A.2: Exploded View of actuator housing.

Part Number	Name of part/materials	Part description	Type
Subassembly 100- Pulley 1			
101	Thinner pulley piece-1	With bearing size middle hole r=76 mm	Manufactured
102	Thinner pulley piece-2	With shaft size middle hole, r=76 mm	
151	Ball bearing	For diameter=0.25'' shaft	Purchased
152	Set screws-1	M4 X 30mm	
153	Locknuts	M4	
Subassembly 200- Pulley 2 and rubber belt			
201	Thinner pulley piece-3	With wire clamp size cable hole	Manufactured
202	Thinner pulley piece-4	With wire diameter cable hole	
203	Flat clamp	Plastic clamp used to fix rubber belt	
204	Rubber belt	Provide elastic force	
152	Set screws-1	Connect pulley 2, M4 X 30 mm	Purchased
153	Locknuts	M4	
252	Set screws-2	Connect pulley 2 and pulley 3, M4 X 40mm	
253	Set screws-3	Fix rubber belt, fully threaded M4 X 30 mm	
Subassembly 300- Pulley 3			
301	Thinner pulley piece-5	With wire diameter cable hole, r=29 mm	Manufactured
302	Thinner pulley piece-6	The same with shoulder pulley, r=25mm	
303	Thinner pulley piece-7	r= 29 mm	
351	Set screws-4	Connect pulley 3, M4 X 14 mm	Purchased
352	Wire	Cable connects actuator and shoulder pulley	
252	Set screws-2	Connect pulley 2 and pulley 3, M4 X 40 mm	
153	Locknuts	M4	

Table A.2: Table of pulley-rubber structure.

Tables(A.2) and (A.1) contain the components specification for purchased and manufactured parts.

Appendix B

Appendix B: Experimental Testing of Polymers

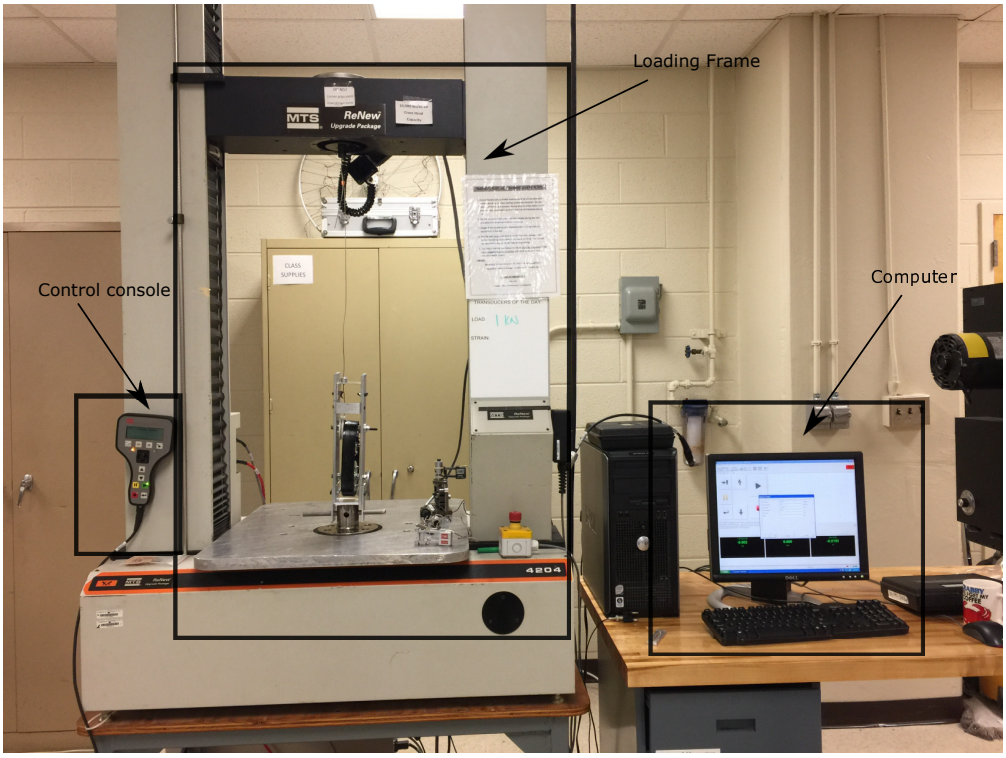

Figure B.1: Instron Machine 4204 from MTS.

The tests about rubber belt and the actuator were implemented on an Instron machine as shown in Figure B.1. The test equipment is Instron machine 4204 from MTS with the maximum load of 1 kN. The whole test instrument can be divided into three parts: the loading frame, containing the testing area which is used to run simple tensile and compressive loading experiments; the control console, containing keys allow operator to easily control the tests; and the computer, working as a peripheral recording device that used to collect, store, and handle all the data.

B.1 Test Procedures

B.1.1 Material Tests

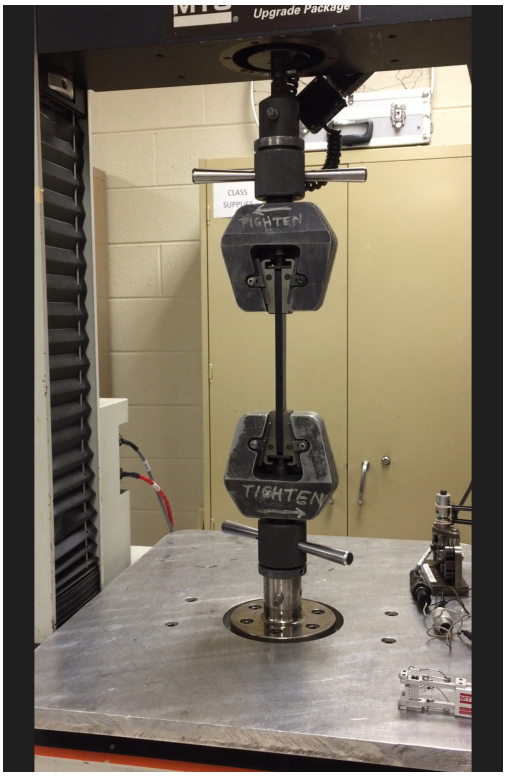

Figure B.2: Test of Polyurethane Belt

To test the polyurethane material and actuator, different test procedures were developed. Due to specific information about the selected 9 kinds of materials were unknown, and the calculations from Chapter 2 were used to roughly determine the dimensions of rubber belt, which required accurate simulations for results discussions. These were the main reasons why material property tests were important. In Figure B.2, upper and lower grip coupling were connecting with wedge action grips. Both ends of the sample belt were clutched and fully inserted into the grips, and left a length of 110 to 120 mm in between. The stretching speed and return speed were the same with 70 mm/min. Every sample belt was stretched to the strain of 10%, 26%, 50%, and 100% and returned to the original position. All the data were collected and stored in computer. All sample belts were operated with the same process.

B.1.2 Material Test of Polymer 9

Different from other 8 kinds of belt samples in the material tests, the polymer 9 sample belt was acquired before the others and so was tested twice. The Figure B.3 depicts the first test results. In the test, both ends of the test belt were fully inserted into the grips, and left a length of 110 mm in between. The cross-section of the belt was 1/16" thick and 1" wide. The energy loss is around 24.5%. Notably, this is much larger than the energy loss found in the second round of testing. The same polymer sample was used in both tests. It is unknown why the results are so different between the two tests.

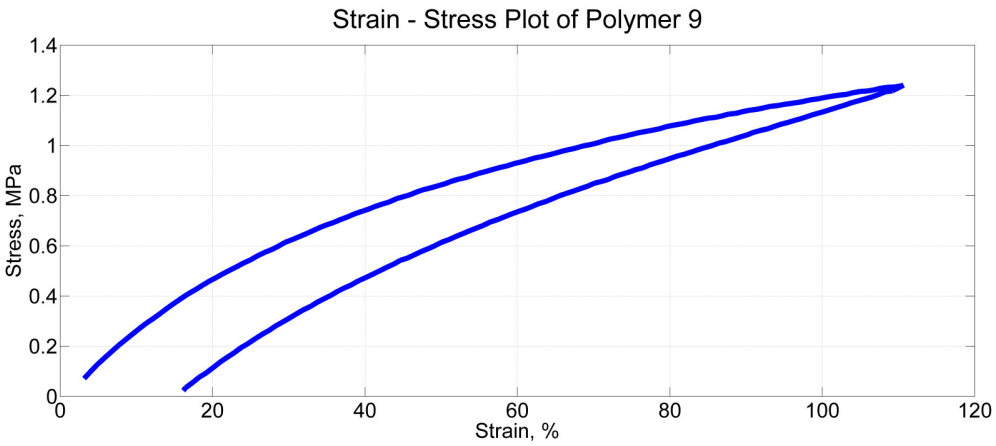

Figure B.3: Test results of Polymer 9 before the final material tests

B.2 Problems and solutions

During the actuator testing process, several unusual conditions occurred, which indicated some of the initial problems with the actuator. The first problem was that the components of pulley 3 came loose and the cable became wedged between some of the layers of pulley 3. The problem was solved when the components of pulley 3 were tightened.

The second problem was interference between pulley 2 and the screws holding on the stop piece. As depicted in Figure B.5, what can be observed from the plots was that when the cable end was pulled up and pulley 2 rotated nearly 150°, there was a sudden stop. Pulley 2 was not stopped by the stop piece but instead by the locknuts of the screws holding on the stop piece. After changing the orientation of those screws, this problem was solved.

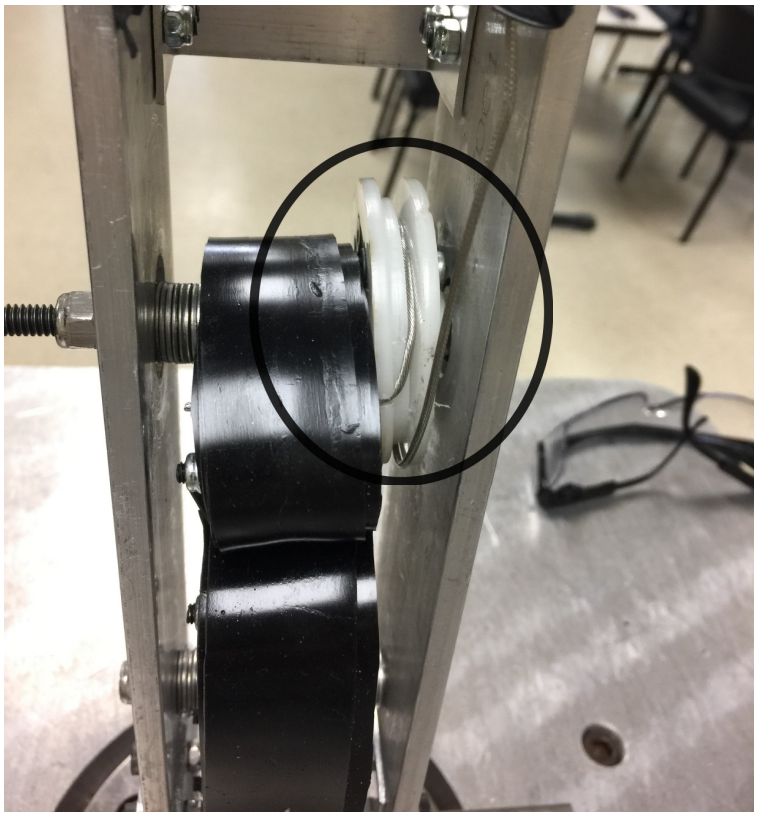

Figure B.4: Cable wedged into pulley 3

Figure B.5: Interference during the test